

Studies on some ternary oxyborates of the $\text{Na}_2\text{O}-\text{Me}_2\text{O}_3-\text{B}_2\text{O}_3$ (Me = rare earth or aluminum) systems: Synthesis, structure and crystal growth

P. Peshev^{a,*}, S. Pechev^b, V. Nikolov^a, P. Gravereau^b, J.-P. Chaminade^b, D. Binev^a,
D. Ivanova^a

^a*Institute of General and Inorganic Chemistry, Bulgarian Academy of Sciences, Acad. G. Bonchev Street, Building 11, 1113 Sofia, Bulgaria*

^b*Institut de Chimie de la Matière Condensée de Bordeaux (ICMCB), CNRS (UPR 9048), Université Bordeaux 1, 87 avenue du Docteur A. Schweitzer, 33608 Pessac, France*

Received 25 August 2005; received in revised form 24 November 2005; accepted 16 January 2006

Available online 13 February 2006

Abstract

Sodium rare-earth oxyborates $\text{Na}_2\text{RE}_2\text{O}(\text{BO}_3)_2$ ($\text{RE} = \text{Y, Nd, Er}$) were prepared for the first time in the present study. They were found to be isostructural with phases of the same composition containing Sm, Eu or Gd and reported by Corbel et al. [J. Solid State Chem. 144 (1999) 35–44]. It was shown that the yttrium and erbium compounds could be synthesized at 900–1000 °C by a solid-state reaction between oxides in an equimolecular ratio. With both oxyborates melting led to decomposition into a mixture of $\text{Y}(\text{Er})\text{BO}_3$, $\text{Y}_2(\text{Er}_2)\text{O}_3$ and $\text{Na}_2\text{B}_4\text{O}_7$. Just the opposite was observed during thermal treatment of the oxide mixture containing Nd_2O_3 , from which a practically pure phase of $\text{Na}_2\text{Nd}_2\text{O}(\text{BO}_3)_2$ was only obtained after melting. The attempts to synthesize the oxyborate $\text{Na}_2\text{La}_2\text{O}(\text{BO}_3)_2$ showed it to be unstable, this leading to the formation of a mixture containing, in addition to $\text{Na}_2\text{La}_2\text{O}(\text{BO}_3)_2$, also other already known stable phases of the system $\text{Na}_2\text{O}-\text{La}_2\text{O}_3-\text{B}_2\text{O}_3$ along with an unknown ternary oxide phase. This phase was found to represent a new oxyborate of sodium and lanthanum with the formula $\text{Na}_3\text{La}_9\text{O}_3(\text{BO}_3)_8$, whose single crystals were obtained by flux growth. It was established that synthesis of a polycrystalline material with the same composition was also possible using solid-state interaction between Na_2CO_3 , La_2O_3 and H_3BO_3 at 1000–1100 °C. X-ray diffraction experiments on single crystals were used to solve the structure of $\text{Na}_3\text{La}_9\text{O}_3(\text{BO}_3)_8$. The unit cell was found to be hexagonal, space group $P62m$ (No. 189) with $Z = 1$. The compound can be regarded as the forefather of a second group of oxyborates representing a new family of isostructural compounds, $\text{Na}_3\text{RE}_9\text{O}_3(\text{BO}_3)_8$. Such phases were obtained with $\text{RE} = \text{Nd, Sm}$ and Eu whereas with $\text{RE} = \text{Y}$ and Gd , the synthesis experiments failed.

The concentration and temperature regions of crystallization of the double-oxyborate $\text{Na}_2\text{Al}_2\text{O}(\text{BO}_3)_2$ in the ternary system $\text{Na}_2\text{O}-\text{Al}_2\text{O}_3-\text{B}_2\text{O}_3$ were determined. This compound was shown to melt incongruently at 970 ± 3 °C, which made high-temperature solution growth most appropriate for obtaining its single crystals with NaBO_2 as the best solvent. On the basis of the data obtained, a composition of the initial solution was proposed, the validity of the choice being demonstrated by the growth of $\text{Na}_2\text{Al}_2\text{O}(\text{BO}_3)_2$ single crystals on a seed using the top-seeded solution growth (TSSG) technique and slow cooling of the solution.

© 2006 Elsevier Inc. All rights reserved.

Keywords: Oxyborates; Crystal structure; Solid-state synthesis; Flux growth; Rare earths; Aluminum

1. Introduction

The foundations of borate crystal chemistry were established some 70 years ago when Zachariasen and Ziegler [1], Zachariasen [2,3], Goldschmidt and Hauptmann [4] and

Fang [5] published the results of the first investigations on borate crystal structures. Since then a great diversity of new structures, which may perhaps exceed even that of the silicate family, have been found. At present over 800 borate crystal structures have been determined [6,7].

The diversity and versatility of borate structures due to the flexibility of boron to adopt either trigonal or tetrahedral oxygen coordination are probably the cause

*Corresponding author. Fax: +359 28705024.

E-mail address: ppeshev@svr.igic.bas.bg (P. Peshev).

of the great variety of properties in borates. Thus, in a series of these compounds, the structural characteristics of the boron–oxygen groups determine their enhanced UV transparency which, combined with a high polarizability and resistance against radiation-induced damage, implies that many borates are attractive candidates for laser hosts and nonlinear optical (NLO) materials with harmonic generation applications [8–12]. Borates are also interesting as promising lithium-ion battery electrode materials [13–18] and ion conductors [19–21]. Some of them have specific magnetic [22,23] and superconducting [24] properties. Recently, borates with a tunnel structure were proposed as basic substances in the development of non-siliceous frameworks for separations and storage as well as in heterogeneous catalysis [25].

The present paper reviews some results obtained recently by the authors in the framework of a program of investigations on $\text{Na}_2\text{O}-\text{Me}_2\text{O}_3-\text{B}_2\text{O}_3$ ($\text{Me} = \text{RE}$ or Al) oxide systems. They concern the following ternary oxyborate phases which appear in these systems: (i) sodium rare-earth oxyborates, $\text{Na}_2\text{RE}_2\text{O}(\text{BO}_3)_2$; (ii) sodium rare-earth oxyborates, $\text{Na}_3\text{RE}_9\text{O}_3(\text{BO}_3)_8$ and (iii) sodium aluminum oxyborate, $\text{Na}_2\text{Al}_2\text{O}(\text{BO}_3)_2$ [26–29].

2. Studies on oxyborates of the $\text{Na}_2\text{RE}_2\text{O}(\text{BO}_3)_2$ family

In 1999, Corbel et al. [30] evidenced the existence of a family of sodium rare-earth oxyborates, $\text{Na}_2\text{RE}_2\text{O}(\text{BO}_3)_2$, with $\text{RE} = \text{Sm}$, Eu and Gd . The authors found all the three compounds obtained by solid-state interaction in equimolar oxide mixtures to be isostructural. Single-crystal X-ray diffraction of a $\text{Na}_2\text{Gd}_2\text{O}(\text{BO}_3)_2$ sample showed it to have a monoclinic structure (S.G. $P2_1/c$, $Z = 4$), the three-dimensional network consisting of infinite sheets of REO_8 polyhedra in the (b, c) plane, which are separated by sodium ions.

The three oxyborates mentioned above contain rare-earth metals (Sm , Eu and Gd) which occupy neighbouring places in the series of lanthanoids in the Periodic Table and have very close values of the RE^{3+} ionic radii. In our study we tested the possibility of synthesizing $\text{Na}_2\text{RE}_2\text{O}(\text{BO}_3)_2$ oxyborates with rare earths having larger and smaller ionic radii than those of samarium, europium and gadolinium. As competitive reactions, yielding Na_3BO_3 , rare-earth borates, REBO_3 , and quaternary phases with the compositions $\text{Na}_3\text{RE}(\text{BO}_3)_2$, $\text{Na}_3\text{RE}_2(\text{BO}_3)_3$ and $\text{Na}_{18}\text{RE}(\text{BO}_3)_7$ [31–33] could also take place, it was of interest to find the conditions of formation of $\text{Na}_2\text{RE}_2\text{O}(\text{BO}_3)_2$ samples with a maximum phase purity.

The preparation of oxyborates with yttrium, lanthanum, neodymium or erbium, respectively, as a rare-earth metal was studied. The four metals were chosen for two reasons: (i) on the basis of their ionic radius size, two of them, Y and Er , having radii RE^{3+} much smaller than the other two, La and Nd , larger than $\text{RE}_{\text{Sm}}^{3+}$, $\text{RE}_{\text{Eu}}^{3+}$ or $\text{RE}_{\text{Gd}}^{3+}$; (ii) on the basis of their possible application, e.g. as optical crystal hosts. Then the sodium yttrium and sodium lanthanum

oxyborates, similarly to the sodium gadolinium oxyborate [30], should be the matrix while the neodymium- and erbium-containing oxyborates should be activators.

For the sake of comparison, experiments on the synthesis of the compound $\text{Na}_2\text{Gd}_2\text{O}(\text{BO}_3)_2$ prepared for the first time by Corbel et al. [30] were performed under the conditions of the investigations on Y -, La -, Nd - and Er -containing samples.

2.1. Experimental

The syntheses of the samples were carried out in platinum crucibles using Na_2CO_3 , H_3BO_3 and RE_2O_3 ($\text{RE} = \text{Y}$, La , Nd , Gd , Er) in a stoichiometric ratio. The rare-earth oxides were subjected to preliminary heating at 1000 °C for 4 h in order to decompose hydroxides and carbonates that may be present on the particle surfaces. Homogenized mixtures of the reagents were subjected to threefold thermal treatment at 900 °C for 24 h and a single heating at the same temperature for 48 h, with intermediate grinding between the separate heatings. Further on, three 24 h treatments with intermediate grinding were performed at 900, 1000 and 1050 °C, respectively. After each of the seven stages of solid-state synthesis, the product was subjected to X-ray phase analysis. With each series the sample obtained after the last stage was tested in order to establish the initial and total melting temperatures. Each test was followed by X-ray phase analysis of the corresponding material.

The heat treatments proceeded in a resistance furnace, the desired temperature being maintained with an accuracy of ± 5 °C. The X-ray powder diffraction patterns needed for phase identification of the samples and for structural analysis were obtained using a Philips X'Pert MPD diffractometer with a Bragg-Brentano geometry ($\text{CuK}\alpha$ radiation). Structure refinement was performed by the Rietveld method, the diffraction patterns being analyzed by a whole pattern fitting procedure using the FULLPROF programme [34].

2.2. Results

Following the weight loss of the samples, one can see in all cases that Na_2CO_3 and H_3BO_3 present in the initial reagent mixtures have already completely decomposed to oxides after the first 24 h heating at 900 °C. Simultaneously, differences in the appearance of the samples containing different rare earths became visible with advancing heat treatment. Thus, after a 120 h heating at 900 °C, the highest degree of sintering is observed with the Er-containing samples. The sintering degree changes in the sequence

$$\text{Er} = \text{Gd} > \text{Y} = \text{Nd} > \text{La},$$

the La-containing sample showing only a negligible sintering.

Thermal treatment at 950 °C results in a measurable increase in grain size with samples containing Y , Gd and Er

only. After heating at 1000 °C all samples exhibit an increase in sintering degree. The appearance of some of the samples significantly changes after treatment at 1050 °C. The surface of those containing Y and Er is covered with small needle-like crystals, whereas the particle size of the La-containing specimen displays a visible increase.

The initial and total melting temperatures of the samples subjected to all the seven stages of thermal treatment at 900–1050 °C are given in Table 1. The presence of an interval of temperatures within which the samples melt shows that even if the solid-state interaction leads to the formation of pure $\text{Na}_2\text{RE}_2\text{O}(\text{BO}_3)_2$ oxyborates, they melt incongruently. As is evident from the data, the narrowest (20 °C) range of melting corresponds to the sample containing Nd. Taking into account the accuracy of determination, it can be assumed that this sample melts practically without decomposition.

Table 2 presents the results obtained by determination of the phase composition of the products after different stages of heating. It is obvious that in all experiments the products of solid-state interaction contain phases which are isostructural with the oxyborate $\text{Na}_2\text{Gd}_2\text{O}(\text{BO}_3)_2$ reported by Corbel et al. [30]. When synthesized at 900 °C, this compound contains no impurities. At higher temperatures, traces of GdBO_3 appear in addition to the main phase. The melting of $\text{Na}_2\text{Gd}_2\text{O}(\text{BO}_3)_2$ is accompanied by its decomposition to a mixture of Gd_2O_3 and $\text{Na}_2\text{B}_4\text{O}_7$. Samples containing yttrium and erbium have shown the same behaviour. In the temperature range between 900 and 1000 °C pure $\text{Na}_2\text{Y}_2\text{O}(\text{BO}_3)_2$ and $\text{Na}_2\text{Er}_2\text{O}(\text{BO}_3)_2$ phases containing traces of YBO_3 or ErBO_3 impurities, respectively, can be obtained. Within the above interval of preparation temperatures these impurities practically do

not change in amount which, as estimated on the basis of measurements, is of the order of 4%. The data for 1050 °C indicate the presence of a second admixture of rare-earth oxide, which evidences the beginning of a decomposition process. Complete decomposition occurs after melting of the samples. The products obtained contain no phase of the type $\text{Na}_2\text{Gd}_2\text{O}(\text{BO}_3)_2$. They consist of REBO_3 , RE_2O_3 and $\text{Na}_2\text{B}_4\text{O}_7$.

Quite a different behaviour is observed with the neodymium-containing sample. After all stages of solid-state interaction at 900–1050 °C the products always contain two main phases, $\text{Na}_2\text{Nd}_2\text{O}(\text{BO}_3)_2$ and $\text{Na}_3\text{Nd}_2(\text{BO}_3)_3$, and an impurity of NdBO_3 . However, after melting, X-ray phase analysis indicates the presence of $\text{Na}_2\text{Nd}_2\text{O}(\text{BO}_3)_2$ and traces of $\text{Na}_3\text{Nd}_2(\text{BO}_3)_3$ only, while NdBO_3 lines are absent. This result is in complete agreement with the data in Table 1, according to which the Nd-containing sample melts in fact congruently.

On the basis of the data in Table 2 it may be concluded that of the phases isostructural with $\text{Na}_2\text{Gd}_2\text{O}(\text{BO}_3)_2$ being the subject of this study, only $\text{Na}_2\text{La}_2\text{O}(\text{BO}_3)_2$ cannot be obtained as a relatively pure product either by solid-state synthesis or by melting. Thermal treatment at 900 °C leads to a mixture containing $\text{Na}_3\text{La}_2(\text{BO}_3)_3$ along with $\text{Na}_2\text{La}_2\text{O}(\text{BO}_3)_2$, while already at 950 °C traces of an unknown phase appear. This phase becomes one of the main components in the sample after melting.

The successful synthesis of practically phase pure sodium rare-earth oxyborates of Y and Er, which are isostructural with the corresponding compounds of Sm, Eu and Gd [30], permitted a structural analysis of the newly prepared substances with the use of X-ray powder diffraction data and the Rietveld method. Unfortunately, the quality of our sample of the Nd-containing compound did not allow us to make a good structural refinement, so only refined unit cell parameters for $\text{Na}_2\text{Nd}_2\text{O}(\text{BO}_3)_2$ are presented in this work.

The conditions of both data collection and structural refinement as well as some basic crystallographic data on $\text{Na}_2\text{Y}_2\text{O}(\text{BO}_3)_2$ and $\text{Na}_2\text{Er}_2\text{O}(\text{BO}_3)_2$ are summarized in Table 3. By way of example, Fig. 1 shows comparison between experimental and calculated patterns for the yttrium compound. The presence of traces of $\text{Y}(\text{Er})\text{BO}_3$ as impurity phases in the samples (ticks indexed as 2) has

Table 1
Initial and total melting points of samples with a $\text{Na}_2\text{O}:\text{RE}_2\text{O}_3:\text{B}_2\text{O}_3 = 1:1:1$ molar ratio containing different rare-earth metals

Rare-earth metal	Y	La	Nd	Gd	Er
Initial melting point (°C)	1260	1090	1170	1230	1170
Total melting point (°C)	>1350	1150	1190	1290	1260

Table 2
Phase composition of the samples with a $\text{Na}_2\text{O}:\text{RE}_2\text{O}_3:\text{B}_2\text{O}_3$ molar ratio after different heat treatments

Rare-earth metal	Temperature and duration of the heat treatment					After melting
	900 °C 48 h	900 °C 120 h	950 °C 24 h	1000 °C 24 h	1050 °C 24 h	
Y	1A,3B	1A,3B	1A,3B	1A,3B	1A,3B,4B	3A,4A,5A
La	1A,2A	1A,2A	1A,2A,6B	1A,2A,3B,6B	1A,2A,3B,6B	1A,2A,6A
Nd	1A,2A,3B	1A,2A,3B	1A,2A,3B	1A,2A,3B	1A,2A,3B	1A,2B
Gd	1A	1A	1A,3B	1A,3B	1A,3B	1A,4A,5B
Er	1A,3B	1A,3B	1A,3B	1A,3B	1A,3B,4B	3A,4A,5A

1, $\text{Na}_2\text{Gd}_2\text{O}(\text{BO}_3)_2$ -type phase [30]; 2, $\text{Na}_3\text{RE}_2(\text{BO}_3)_3$ phase; 3, REBO_3 phase; 4, RE_2O_3 phase; 5, $\text{Na}_2\text{B}_4\text{O}_7$; 6, unknown phase; RE = Y, La, Nd, Gd, Er A, main phase; B, traces.

Table 3
Crystallographic data and conditions of powder data collection for $\text{Na}_2\text{RE}_2\text{O}(\text{BO}_3)_2$ ($\text{RE} = \text{Y, Er}$)

	Y	Er
Symmetry	Monoclinic	Monoclinic
Space group	$P2_1/c$	$P2_1/c$
Z	4	4
Temperature (K)	293(2)	293(2)
Cell parameters		
a (Å)	10.5980(3)	10.5757(2)
b (Å)	6.2305(2)	6.2101(1)
c (Å)	10.2244(3)	10.1976(2)
β (deg.)	117.76(2)	117.73(1)
Volume (Å ³)	597.40(6)	592.80(4)
Calculated density (g/cm ³)	3.97	5.76
Date collection range	$8^\circ < 2\theta < 120^\circ$	$8^\circ < 2\theta < 120^\circ$
Step	0.02°	0.02°
Counting time (s/deg.)	30	30
Wavelengths, $\text{CuK}\alpha_{1,2}$ (Å)	1.54056, 1.54439	1.54056, 1.54439
Number of reflections	881	874
Number of refined parameters	65	65
Reliability factors		
R_p	9.51	10.5
R_{wp}	12.4	13.6
R_B	2.78	4.03
χ^2	1.98	3.29

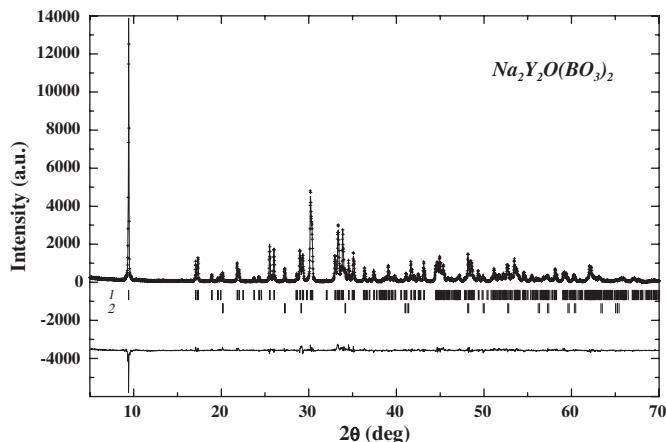


Fig. 1. Experimental (+) and calculated (solid line) X-ray diffraction patterns of $\text{Na}_2\text{Y}_2\text{O}(\text{BO}_3)_2$ and the difference between them 1, main phase, $\text{Na}_2\text{Y}_2\text{O}(\text{BO}_3)_2$; 2, impurity phase, YBO_3 .

been taken into account. Owing to the large number of variables during the refinement, the temperature parameters of the crystallographically distinct boron and oxygen atoms were considered as being identical. The B–O distances were also constrained to the average value of 1.38 Å, determined on a single crystal for the BO_3^{3-} ions in $\text{Na}_2\text{Gd}_2\text{O}(\text{BO}_3)_2$ [30]. The refined atomic coordinates and temperature factors for the two oxyborates are given in Table 4.

The structure of the $\text{Na}_2\text{RE}_2\text{O}(\text{BO}_3)_2$ oxyborates was already described in terms of a three-dimensional network of cation-centered REO_8 , NaO_6 and BO_3 polyhedra [30]. The interatomic distances within some of these polyhedra

Table 4
Atomic coordinates and temperature factors in $\text{Na}_2\text{RE}_2\text{O}(\text{BO}_3)_2$ ($\text{RE} = \text{Y}^a, \text{Er}^b$)

Atom	Site	x	y	z	B_{iso} (Å ²)
$\text{RE}(1)$	4e	^a 0.1835(3)	0.0815(5)	0.0877(3)	0.91(7)
		^b 0.1825(3)	0.0822(4)	0.0874(4)	0.71(1)
$\text{RE}(2)$	4e	^a 0.9842(3)	0.4591(5)	0.1821(3)	0.81(7)
		^b 0.9836(3)	0.4609(6)	0.1821(3)	0.71(1)
$\text{Na}(1)$	4e	^a 0.526(1)	-0.059(2)	0.264(1)	1.6(3)
		^b 0.526(2)	-0.054(3)	0.264(2)	1.0(4)
$\text{Na}(2)$	4e	^a 0.609(1)	0.256(2)	0.046(1)	1.5(3)
		^b 0.608(2)	0.256(4)	0.042(2)	1.6(6)
$\text{O}(1)$	4e	^a 0.972(2)	0.124(3)	0.099(2)	0.9(2)
		^b 0.974(3)	0.138(4)	0.100(2)	0.8(3)
$\text{O}(2)$	4e	^a 0.320(2)	-0.248(3)	0.137(2)	0.9(2)
		^b 0.320(2)	-0.248(4)	0.134(3)	0.8(3)
$\text{O}(3)$	4e	^a 0.170(1)	0.258(3)	0.365(2)	0.9(2)
		^b 0.171(2)	0.260(4)	0.365(3)	0.8(3)
$\text{O}(4)$	4e	^a 0.149(1)	0.458(2)	0.087(2)	0.9(2)
		^b 0.146(3)	0.455(3)	0.087(3)	0.8(3)
$\text{O}(5)$	4e	^a 0.399(2)	0.159(3)	0.057(1)	0.9(2)
		^b 0.397(3)	0.156(4)	0.057(2)	0.8(3)
$\text{O}(6)$	4e	^a 0.853(2)	0.255(2)	0.275(2)	0.9(2)
		^b 0.854(3)	0.252(4)	0.276(3)	0.8(3)
$\text{O}(7)$	4e	^a 0.368(2)	0.149(2)	0.335(2)	0.9(2)
		^b 0.367(3)	0.146(4)	0.335(3)	0.8(3)
$\text{B}(1)$	4e	^a 0.318(1)	0.257(5)	-0.077(2)	1.2(5)
		^b 0.318(2)	0.257(1)	-0.077(4)	2.1(9)
$\text{B}(2)$	4e	^a 0.208(3)	-0.344(3)	0.147(3)	1.2(5)
		^b 0.206(4)	-0.343(6)	0.144(12)	2.1(9)

in the Y and Er compounds are summarized in Table 5. According to this description the O1 atom occupies a particular position since it is not bonded to any of the above polyhedra. Moreover, it is associated with the shortest RE–O distances in these compounds. So it is worth examining the structure from the point of view of oxocentered polyhedra. Fig. 2 shows that O1 participates in ORE_4 tetrahedra. These tetrahedra share a common edge so as to form O_2RE_6 finite units which are corner linked and result in a two-dimensional layer of oxygen-centered rare-earth tetrahedra in the bc -plane. The average O1–Y and O1–Er distances are 2.276(8) and 2.27(1) Å, which is very close to the predicted values 2.276 and 2.245 Å, respectively, for four coordinated O^{2-} ions with Y^{3+} or Er^{3+} [35]. Bond-valence calculations were performed. They revealed no significant deviations from the theoretical values; the results are available on demand from the authors.

During the preparation of this paper, two studies reported relevant results. Thus, Heymann et al. [36] published data on solid-state synthesis at 900–950 °C of two new oxyborates, $\text{Na}_2\text{RE}_2\text{O}(\text{BO}_3)_2$ ($\text{RE} = \text{Dy, Ho}$) isotypic to the phases which are the subject of the present work and of the study of Corbel et al. [30]. The second investigation [37] confirmed our results reported previously in Ref. [26] concerning the structure parameters of $\text{Na}_2\text{Y}_2\text{O}(\text{BO}_3)_2$. The authors established that doping of

Table 5
Selected distances (Å) and angles (deg.) in $\text{Na}_2\text{RE}_2\text{O}(\text{BO}_3)_2$ ($\text{RE} = \text{Y, Er}$)

$\text{Na}_2\text{Y}_2\text{O}(\text{BO}_3)_2$							
$\text{Y}(1)-\text{O}(1)$	2.24(1)	$\text{Y}(2)-\text{O}(1)$	2.24(2)	$\text{B}(1)-\text{O}(7)$	1.37(3)	$\text{O}(7)-\text{B}(1)-\text{O}(5)$	126(2)
$\text{Y}(1)-\text{O}(1)$	2.31(2)	$\text{Y}(2)-\text{O}(1)$	2.31(2)	$\text{B}(1)-\text{O}(5)$	1.37(2)	$\text{O}(5)-\text{B}(1)-\text{O}(3)$	116.7(2)
$\text{Y}(1)-\text{O}(4)$	2.37(1)	$\text{Y}(2)-\text{O}(3)$	2.35(1)	$\text{B}(1)-\text{O}(3)$	1.39(2)	$\text{O}(3)-\text{B}(1)-\text{O}(7)$	117(2)
$\text{Y}(1)-\text{O}(7)$	2.40(1)	$\text{Y}(2)-\text{O}(4)$	2.36(2)	$\langle \text{B}-\text{O} \rangle$	1.38		
$\text{Y}(1)-\text{O}(2)$	2.42(2)	$\text{Y}(2)-\text{O}(3)$	2.38(2)	$\text{B}(2)-\text{O}(2)$	1.38(4)	$\text{O}(2)-\text{B}(2)-\text{O}(4)$	125(2)
$\text{Y}(1)-\text{O}(3)$	2.43(2)	$\text{Y}(2)-\text{O}(6)$	2.39(2)	$\text{B}(2)-\text{O}(6)$	1.38(4)	$\text{O}(4)-\text{B}(2)-\text{O}(6)$	115(2)
$\text{Y}(1)-\text{O}(5)$	2.49(2)	$\text{Y}(2)-\text{O}(6)$	2.42(2)	$\text{B}(2)-\text{O}(4)$	1.39(2)	$\text{O}(6)-\text{B}(2)-\text{O}(2)$	120(3)
$\text{Y}(1)-\text{O}(6)$	2.60(2)	$\text{Y}(2)-\text{O}(4)$	2.49(2)				
$\langle \text{Y}(1)-\text{O} \rangle = 2.41$		$\langle \text{Y}(2)-\text{O} \rangle = 2.37$					
$\text{Na}_2\text{Er}_2\text{O}(\text{BO}_3)_2$							
$\text{Er}(1)-\text{O}(1)$	2.28(4)	$\text{Er}(2)-\text{O}(1)$	2.16(3)	$\text{B}(1)-\text{O}(7)$	1.37(6)	$\text{O}(7)-\text{B}(1)-\text{O}(5)$	128(4)
$\text{Er}(1)-\text{O}(1)$	2.30(2)	$\text{Er}(2)-\text{O}(1)$	2.33(3)	$\text{B}(1)-\text{O}(5)$	1.37(4)	$\text{O}(5)-\text{B}(1)-\text{O}(3)$	115(3)
$\text{Er}(1)-\text{O}(4)$	2.35(2)	$\text{Er}(2)-\text{O}(4)$	2.33(3)	$\text{B}(1)-\text{O}(3)$	1.39(3)	$\text{O}(3)-\text{B}(1)-\text{O}(7)$	117(4)
$\text{Er}(1)-\text{O}(7)$	2.40(2)	$\text{Er}(2)-\text{O}(3)$	2.35(2)	$\langle \text{B}-\text{O} \rangle$	1.38		
$\text{Er}(1)-\text{O}(3)$	2.42(3)	$\text{Er}(2)-\text{O}(3)$	2.37(4)	$\text{B}(2)-\text{O}(2)$	1.38(7)	$\text{O}(2)-\text{B}(2)-\text{O}(4)$	126(5)
$\text{Er}(1)-\text{O}(2)$	2.43(2)	$\text{Er}(2)-\text{O}(6)$	2.38(3)	$\text{B}(2)-\text{O}(6)$	1.40(5)	$\text{O}(4)-\text{B}(2)-\text{O}(6)$	112(6)
$\text{Er}(1)-\text{O}(5)$	2.47(3)	$\text{Er}(2)-\text{O}(6)$	2.39(3)	$\text{B}(2)-\text{O}(4)$	1.37(9)	$\text{O}(6)-\text{B}(2)-\text{O}(2)$	121(7)
$\text{Er}(1)-\text{O}(6)$	2.61(3)	$\text{Er}(2)-\text{O}(4)$	2.49(3)				
$\langle \text{Er}(1)-\text{O} \rangle = 2.41$		$\langle \text{Er}(1)-\text{O} \rangle = 2.35$					

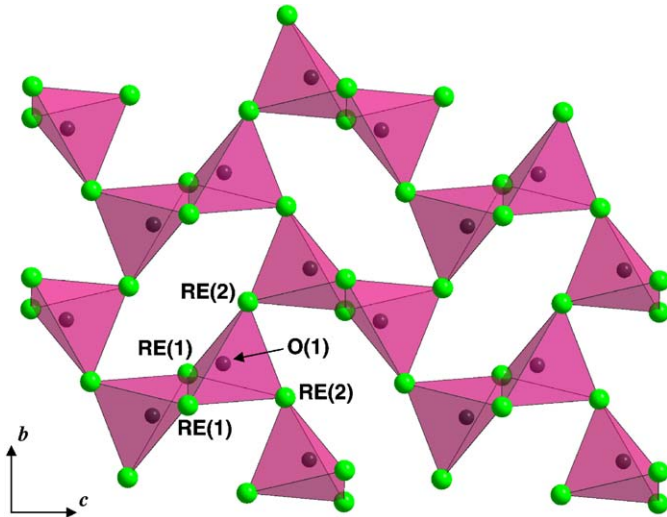


Fig. 2. View showing the formation in $\text{Na}_2\text{RE}_2\text{O}(\text{BO}_3)_2$ of a two-dimensional layer of oxygen-centered RE tetrahedra in the bc -plane.

this compound with Eu^{3+} ions led to a strong red emission of the $^5\text{D}_0-^7\text{F}_2$ transition at 611 nm.

The cell parameters of Y-, Nd- and Er-containing oxyborates determined in this study are listed in Table 6. For the sake of comparison the parameters of the compounds with Y, Sm, Eu, Gd, Dy and Ho given in Refs. [30,36,37] are also presented. It is evident that the change in lattice parameters is in agreement with evolution of the ionic radii R_i^{3+} of the rare earths [38].

3. Studies on oxyborates of the $\text{Na}_3\text{RE}_9\text{O}_3(\text{BO}_3)_8$ family

As was pointed out above, attempts to prepare $\text{Na}_2\text{La}_2\text{O}(\text{BO}_3)_2$ as a pure phase by solid-state interaction

between oxides at different temperatures failed. After melting the product consisted of $\text{Na}_2\text{La}_2\text{O}(\text{BO}_3)_2$ -type borate, $\text{Na}_3\text{La}_2(\text{BO}_3)_3$ and an unknown ternary oxide phase. Determination of the chemical composition showed this phase to correspond to a ternary borate with the formula $\text{Na}_3\text{La}_9\text{O}_3(\text{BO}_3)_8$. This oxyborate was prepared without admixtures of other phases by solid-state interaction at 1000 and 1100 °C with several intermediate grindings of a pelletized initial mixture of Na_2CO_3 , La_2O_3 and H_3BO_3 in a stoichiometric molar ratio.

3.1. Crystal growth of $\text{Na}_3\text{La}_9\text{O}_3(\text{BO}_3)_8$ and determination of its structure

Single crystals of $\text{Na}_3\text{La}_9\text{O}_3(\text{BO}_3)_8$ were grown by spontaneous crystallization on platinum rods immersed in melts of the constituent binary oxides during their cooling with a rate of 1 °C/h. The experiments were carried out in a resistance furnace with SiC heating elements. The melts were prepared in Pt crucibles, starting compositions with a constant B_2O_3 content (33.3 mol%) being used. In the equilibrium diagram they were situated on the line corresponding to a Na_2O content between 33.3 and 40.0 mol% and a La_2O_3 content varying in the concentration range 33.3–26.7 mol%. The crystallization temperature changed from 1150 to 1100 °C with increasing Na_2O content. It is evident that $\text{Na}_3\text{La}_9\text{O}_3(\text{BO}_3)_8$ crystallizes in a region of the $\text{Na}_2\text{O}-\text{La}_2\text{O}_3-\text{B}_2\text{O}_3$ ternary diagram richer in Na_2O than the phase itself, the neighbouring regions being the $\text{Na}_3\text{La}_2(\text{BO}_3)_3$ region (with a higher B_2O_3 content) and the $\text{Na}_2\text{La}_2\text{O}(\text{BO}_3)_2$ region (with a higher Na_2O content).

The single-crystal X-ray diffraction experiments were carried out on a Nonius Kappa CCD diffractometer using $\text{MoK}\alpha$ radiation. All crystal data and experimental

Table 6

Cell parameters of sodium rare earth oxyborates, $\text{Na}_2\text{RE}_2\text{O}(\text{BO}_3)_2$

Oxyborate	<i>a</i> (Å)	<i>b</i> (Å)	<i>c</i> (Å)	β (°C)	<i>V</i> (Å ³)	R_{f}^{3+} (Å) [38]	Source
$\text{Na}_2\text{Y}_2\text{O}(\text{BO}_3)_2$	10.5980(3)	6.2305(2)	10.2244(2)	117.76(2)	597.40(6)	1.019	This work
$\text{Na}_2\text{Y}_2\text{O}(\text{BO}_3)_2$	10.5993(1)	6.2311(1)	10.2247(1)	117.756(1)	597.59(3)	1.019	[37]
$\text{Na}_2\text{Nd}_2\text{O}(\text{BO}_3)_2$	10.8204(7)	6.4297(6)	10.4617(9)	117.96(3)	642.87(9)	1.019	This work
$\text{Na}_2\text{Sm}_2\text{O}(\text{BO}_3)_2$	10.754(2)	6.369(2)	10.381(2)	117.85(2)	628.6(2)	1.079	[30]
$\text{Na}_2\text{Eu}_2\text{O}(\text{BO}_3)_2$	10.721(7)	6.343(6)	10.347(7)	117.84(5)	622.1(6)	1.066	[30]
$\text{Na}_2\text{Gd}_2\text{O}(\text{BO}_3)_2$	10.695(6)	6.320(4)	10.328(6)	117.80(4)	617.5(9)	1.053	[30]
$\text{Na}_2\text{Dy}_2\text{O}(\text{BO}_3)_2$	10.639(1)	6.262(1)	10.253(1)	117.76(1)	604.95(3)	1.027	[36]
$\text{Na}_2\text{Ho}_2\text{O}(\text{BO}_3)_2$	10.612(5)	6.237(2)	10.225(3)	117.7(1)	599.20(3)	1.015	[36]
$\text{Na}_2\text{Er}_2\text{O}(\text{BO}_3)_2$	10.5757(2)	6.2101(1)	10.1976(2)	117.73(1)	592.80(4)	1.004	This work

Table 7

Crystal data and structure refinement for $\text{Na}_3\text{La}_9\text{O}_3(\text{BO}_3)_8$ *Crystal data*

Empirical formula	$\text{Na}_3\text{La}_9\text{O}_3(\text{BO}_3)_8$
Formula weight	1837.64 g
Crystal system	Hexagonal
Space group	<i>P-6 2m</i> (No. 189)
Temperature (K)	293(2)
Unit cell dimensions (from 1182 reflections with $\theta = 1.0\text{--}30.0^\circ$) (Å)	$a = b = 8.9033(3)$ $c = 8.7131(3)$
Volume (Å ³)	598.14(4)
<i>Z</i>	1
D_m (by hydrostatic pressure meas. in $\text{C}_6\text{H}_5\text{Br}$) (Mg m ⁻³)	5.06(2)
D_x (Mg m ⁻³)	5.102
$F(000)$	802
Crystal shape	Wedge-shaped plate
Crystal colour	Transparent colourless
Crystal size (mm ³)	0.220 × 0.060 × 0.040

Data collection

Diffractometer	Nonius Kappa CCD
Collect	ϕ/ω scan
Radiation	$\text{MoK}\alpha$ ($\lambda = 0.71073$ Å)
Absorption coefficient (mm ⁻¹)	15.9
θ range (deg.)	3.5–30.0
Index ranges	$-12 \leq h \leq 12$ $-12 \leq k \leq 12$ $-12 \leq l \leq 12$

Reflections collected [$I > 2\sigma(I)$]Independent reflections [$I > 2\sigma(I)$]
(Friedel not merged)*Refinement*

Absorption correction

Refinement method

Data/parameters refined

Weighting scheme

Extinction coefficient

Goodness-of-fit on F^2 Final *R* indices [$I > 2\sigma(I)$]

Absolute structure parameter

Largest diff. peak and hole (eÅ⁻³)

Empirical, Scalepack
$T_{\text{min}} = 0.150$; $T_{\text{max}} = 0.540$
Full-matrix least-squares on F^2
684/49
$\omega = 1/$
$[\sigma^2(F_o^2) + (0.0165P)^2 + 0.07P]$
where $P = (F_o^2 + 2F_c^2)/3$
0.054(1)
1.24
$R_1 = 0.015$, $wR_2 = 0.030$
$-0.03(3)$
1.25 (on La1 site) and -1.78

conditions in $\text{Na}_3\text{La}_9\text{O}_3(\text{BO}_3)_8$ structure determination are summarized in Table 7. The test of equivalent data merging in the different possible Laue classes indicates good

Table 8

Atomic coordinates and equivalent isotropic displacement parameters (Å²) for $\text{Na}_3\text{La}_9\text{O}_3(\text{BO}_3)_8$. $U(\text{eq})$ is defined as one third of the trace of the orthogonalized U_{ij} tensor

Atom	Site	<i>x</i>	<i>y</i>	<i>z</i>	<i>U</i> (eq)
La1	3 <i>g</i>	0.28323(4)	0.28323(4)	1/2	0.0051(1)
La2	6 <i>i</i>	0.34806(2)	0	0.23333(2)	0.0056(1)
Na	3 <i>f</i>	0.3366(2)	0.3366(2)	0	0.0145(7)
B1	2 <i>e</i>	0	0	0.2084(8)	0.0075(14)
B2	2 <i>c</i>	2/3	1/3	0	0.0063(15)
B3	4 <i>h</i>	2/3	1/3	0.3234(6)	0.0072(10)
O1	6 <i>i</i>	0.1558(3)	0.1558(3)	0.2120(3)	0.0102(5)
O2	6 <i>j</i>	0.5047(4)	0.1824(4)	0	0.0092(5)
O3	12 <i>l</i>	0.5129(3)	0.3334(2)	0.3171(2)	0.0098(4)
O4	3 <i>g</i>	0.2572(4)	0	1/2	0.0075(7)

agreement with the hexagonal 6/mmm Laue class ($R_{\text{int}} = 0.040$).As no particular reflection conditions were observed in the data set, five possible space groups had to be considered: *P6/mmm*, *P-6m2*, *P-62m*, *P6mm* and *P622*. After several trials the structure was solved by Patterson function deconvolution and the heavy atom method in the *P-62m* non-centric space group. At first, two sites for the lanthanum and one site for the sodium atoms were located (SHELXS-86 program [39]). Then the boron and oxygen positions in the structure were obtained by refinement and successive Fourier difference functions (SHELXL-93 program [40]). The final results on the atomic coordinates, equivalent isotropic displacements and anisotropic displacements parameters are indicated in Tables 8 and 9. Selected interatomic distances and angles are listed in Table 10.3.2. Structure description of $\text{Na}_3\text{La}_9\text{O}_3(\text{BO}_3)_8$ In a general manner the crystallographic structure of $\text{Na}_3\text{La}_9\text{O}_3(\text{BO}_3)_8$ can be described as a layer-type structure, since there is alternate stacking along the *c*-axis of: $\text{Na}_2\text{B}_2(\text{O}_2)_3$ ($z = 0$); $\text{B}_1(\text{O}_1)_3$ ($z = 0.21$); La_2 ($z = 0.23$); $\text{B}_3(\text{O}_3)_3$ ($z = 0.32$); La_1O_4 on the mirror plane at $z = 1/2$ (Fig. 3).

The description can be done on the basis of the near “compact stacking” of the Na, La cations and the usual *A*, *B*, *C* compact planes notation. So, if Na ions (*z* = 0) form an *A*-type plane, La2-ions (*z* = 0.23) are a *B*-type plane and La1-ions (*z* = 1/2) are again in an *A*-type plane, then the stacking of Na and La cations on the sequence *ABAB* ...

Table 9

Anisotropic displacement parameters (Å^2) for $\text{Na}_3\text{La}_9\text{O}_3(\text{BO}_3)_8$. The anisotropic displacement factor exponent takes the form: $-2\pi^2(h^2a^2U_{11} + \dots + 2hka*b*U_{12} + \dots)$

	U_{11}	U_{22}	U_{33}	U_{23}	U_{13}	U_{12}
La1	0.0052(2)	0.0052(2)	0.0055(2)	0	0	0.0032(2)
La2	0.0058(1)	0.0057(1)	0.0052(1)	0	0.0006(1)	0.0028(1)
Na	0.011(1)	0.011(1)	0.021(2)	0	0	0.006(1)
B1	0.009(2)	0.009(2)	0.005(3)	0	0	0.004(1)
B2	0.008(2)	0.008(2)	0.002(3)	0	0	0.004(1)
B3	0.009(2)	0.009(2)	0.004(2)	0	0	0.004(1)
O1	0.008(1)	0.008(1)	0.013(1)	-0.001(1)	-0.001(1)	0.003(1)
O2	0.007(1)	0.010(1)	0.008(1)	0	0	0.002(1)
O3	0.009(1)	0.009(1)	0.013(1)	0.000(1)	0.001(1)	0.005(1)
O4	0.009(1)	0.009(2)	0.004(2)	0	0	0.005(1)

will be hexagonal compact (h.c.) (Fig. 4). Within this description, the BO_3 triangles are arranged in rows running along the *c*-axis and they could be projected in the *C* positions of the compact packing. We can distinguish between two types of BO_3 rows: type 1, with “eclipsed” triangles (two BO_3 per cell in (0, 0) projection) and type 2, with a succession of two “eclipsed” and one “rotated” triangle (six BO_3 per cell in (1/3, 2/3) and (2/3, 1/3) projections. A similar kind of structure can be found for $\text{Hg}_3(\text{BO}_3)_2$. One can compare $[\text{Na}_3\text{La}_9(\text{BO}_3)_8$ with $\text{Hg}_{12}(\text{BO}_3)_8$, which also has an *ABAB* ... h.c. network of Hg atoms and rows of “rotated” BO_3 triangles in *C* positions, parallel to the *c*-axis [41].

The O4 atoms, which are independent of the BO_3 triangles and justify the oxyborate label of the compound are on the mirror plane (*z* = 1/2) in tetrahedral sites of a *B*–*A*–*B* lanthanum “compact sandwich”.

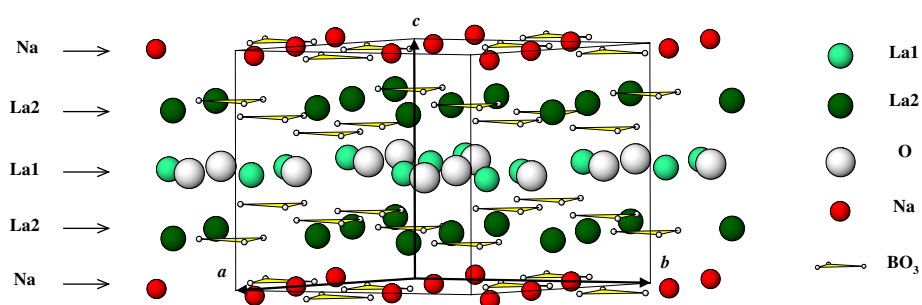
Another description of the framework can be done using the above O_4La_4 tetrahedra. Three tetrahedra share a common La corner and constitute a La_9O_3 ring parallel to the (*ab*) plane (Fig. 5). The rings are separated by Na – $\text{B}_2(\text{O}_2)_3$ planes and BO_3 rows of type 2. The BO_3 rows of type 1 run inside the rings.

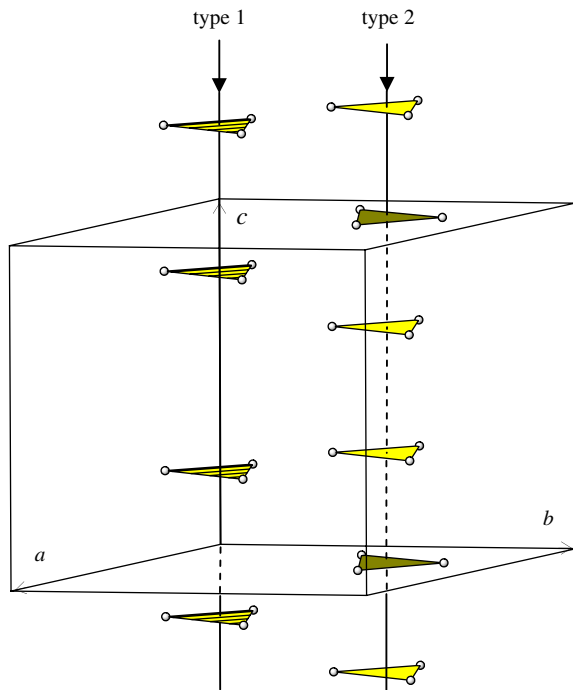
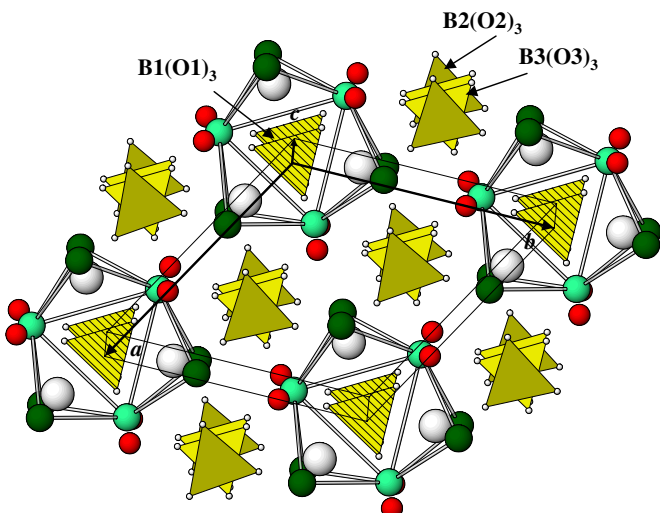
Table 10

Selected bond lengths (\AA) and angles (deg) in $\text{Na}_3\text{La}_9\text{O}_3(\text{BO}_3)_8$

La1	2 ×	O4 ^I	2.414(2)	La2	O4	2.460(2)
	4 ×	O3 ^{II, III, IV}	2.450(2)		O2 ^V	2.540(2)
	2 ×	O1 ^{III}	2.754(2)		O3 ^{VI, VII}	2.568(2)
Na	2 ×	O1 ^X	2.450(3)	B1	O3 ^{VIII}	2.673(2)
	2 ×	O2 ^{X I}	2.486(3)		O1 ^{IX}	2.695(2)
	2 ×	O2 ^{XII, XIII}	2.632(3)		O1 ^{I, IX}	1.388(3)
O1–Na–O1 ^X			97.85(14)	B2	3 ×	O2 ^{VI, XII}
O1–Na–O2			90.93(6)	O1–B1–O1 ^I		119.95(2)
O1–Na–O2 ^{XII}			123.74(6)			120
O2–Na–O2 ^{XI}			177.2(2)	B3	3 ×	O3 ^{VI, XII}
O2–Na–O2 ^{XII}			56.27(14)	O3–B3–O3 ^{VI}		1.371(3)
O4	2 ×	La1 ^{IX}	2.414(2)			119.84(4)
	2 ×	La2 ^{III}	2.460(2)			
	La1–O4–La1 ^{IX}		129.5(2)			
	La1–O4–La2		98.06(2)			
	La2–O4–La2 ^{III}		141.6(2)			

Symmetry codes: (I) $-y, x-y, z$; (II) $y, x, -z+1$; (III) $x, y, -z+1$; (IV) y, x, z ; (V) $x-y, -y, -z$; (VI) $-y+1, x-y, z$; (VII) $-x+1, -x+y, z$; (VIII) $x-y, -y, z$; (IX) $-x+y, -x, z$; (X) $x, y, -z$; (XI) $y, x, -z$; (XII) $-x+y+1, -x+1, z$; (XIII) $-x+1, -x+y+1, -z$.

Fig. 3. The layer-type structure of $\text{Na}_3\text{La}_9\text{O}_3(\text{BO}_3)_8$.

Fig. 4. View of the two types of BO_3 rows.Fig. 5. View of $\text{Na}_3\text{La}_9\text{O}_3(\text{BO}_3)_8$ along the c -axis. Three O_4La_4 tetrahedra share common corners to form La_9O_3 rings. Types 1 and 2 BO_3 rows run inside and between the rings.

3.2.1. Lanthanum atom environment

Lanthanum atoms occupy two different crystallographic sites: La1 in $3g$ and La2 in $6i$, eight and nine coordinated, respectively (Fig. 6). La–O bond distances range from 2.414(2) to 2.754(2) Å for La1, and from 2.460(2) to 2.695(2) Å for La2. These values are close to those reported for the La–O distances in lanthanum borate, $\text{La}_{26}(\text{BO}_3)_8\text{O}_{27}$ [42].

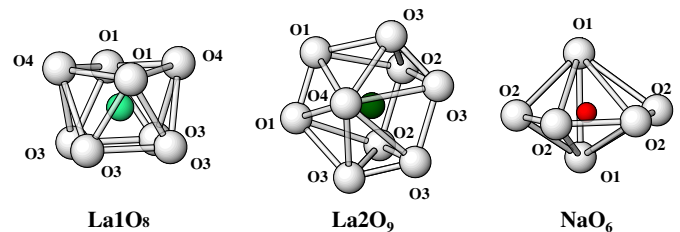


Fig. 6. Coordination polyhedra of the La1, La2 and Na cations.

3.2.2. Boron atom environment

All boron groups consist of a boron triangularly coordinated to oxygen atoms. Three types of crystallographically-independent isolated $(\text{BO}_3)^{3-}$ groups parallel to the (ab) plane are present in the unit cell similarly to the case of other borate and oxyborate compounds [43]. In $\text{Na}_3\text{La}_9\text{O}_3(\text{BO}_3)_8$ only small deviations from the ideal borate group having a B–O distance and O–B–O angle values equal to 1.38 Å and 120°, respectively, are observed (Table 10). For the sake of comparison, it should be noted that the same order of B–O distances has been reported for other borates containing isolated BO_3 triangles, e.g. 1.360–1.399 Å for $\text{LiGd}_6\text{O}_5(\text{BO}_3)_3$ [43] and 1.34–1.42 Å for $\text{La}_{26}(\text{BO}_3)_8\text{O}_{27}$ [42].

3.2.3. Sodium atom environment

The unit cell contains one type of Na atoms only. Sodium is surrounded by six oxygen atoms (two O1 and four O2), forming a highly distorted octahedron (Table 7, Fig. 6).

3.2.4. Oxygen atom environment

Oxygen atoms can be classified into three groups depending on their bonding with other atoms in the unit cell. Thus, O1 and O2 atoms are connected to Na, B and La atoms, O3 to B and La, while O4 are bonded to four La atoms only. The appearance of a Ln –O bonding of the latter type was reported previously for $\text{LiLn}_6\text{O}_5(\text{BO}_3)_3$ ($\text{Ln} = \text{Pr–Tm}$) [43], $\text{Li}_2\text{Ln}_5\text{O}_4(\text{BO}_3)_3$ ($\text{Ln} = \text{Yb, Lu}$) [44] and $\text{Na}_2\text{Ln}_2\text{O}(\text{BO}_3)_2$ ($\text{Ln} = \text{Sm, Eu, Gd}$) [30]. Similarly to these substances, $\text{Na}_3\text{La}_9\text{O}_3(\text{BO}_3)_8$ can be labelled as an oxyborate of sodium and lanthanum. It is worth noting that the La–O4 bond distances belong to the shortest ones (2.414–2.460 Å). The O4 oxygen atoms are located in the four coordinated La_4O tetrahedra mentioned above, which form rings (Fig. 5), the bond distances and angle values being presented in Table 10.

3.3. $\text{Na}_3\text{RE}_9\text{O}_3(\text{BO}_3)_8$ ($\text{RE} = \text{Nd, Sm, Eu}$) oxyborates isostructural with $\text{Na}_3\text{La}_9\text{O}_3(\text{BO}_3)_8$

Solid-phase interactions between Na_2CO_3 , H_3BO_3 and Nd_2O_3 (Sm_2O_3 or Eu_2O_3 , respectively) in a stoichiometric molar ratio under the regime used for the preparation of polycrystalline $\text{Na}_3\text{La}_9\text{O}_3(\text{BO}_3)_8$ were successfully applied to obtaining analogues of this compound containing

Table 11
Cell parameters of sodium rare-earth oxyborates, $\text{Na}_3\text{RE}_9\text{O}_3(\text{BO}_3)_8$

Oxyborate	<i>a</i> (Å)	<i>c</i> (Å)	<i>V</i> (Å ³)	$R_{\text{i}}^{3+}(\text{C.N.})$ [38]
$\text{Na}_3\text{La}_9\text{O}_3(\text{BO}_3)_8^{\text{a}}$	8.903(3)	8.713(3)	598.14(4)	1.160 ^{VIII} ; 1.216 ^{IX}
$\text{Na}_3\text{Nd}_9\text{O}_3(\text{BO}_3)_8$	8.767(1)	8.476(1)	564.2(1)	1.109 ^{VIII} ; 1.163 ^{IX}
$\text{Na}_3\text{Sm}_9\text{O}_3(\text{BO}_3)_8$	8.706(1)	8.359(1)	548.7(1)	1.079 ^{VIII} ; 1.132 ^{IX}
$\text{Na}_3\text{Eu}_9\text{O}_3(\text{BO}_3)_8$	8.682(1)	8.308(1)	542.3(1)	1.066 ^{VIII} ; 1.120 ^{IX}

^aSingle-crystal XRD data.

neodymium, samarium and europium. However, the attempts to synthesize Y- and Gd-containing phases in the same manner, failed.

The X-ray powder diffraction experiments needed for the identification of the new phases and their structural analysis were carried out using the instruments and procedures described in Section 2.1. The cell parameter values obtained by whole pattern refinement of powder XRD data are presented in Table 11, where, for the sake of comparison, data from the single-crystalline structure determination of $\text{Na}_3\text{La}_9\text{O}_3(\text{BO}_3)_8$ are also given.

3.4. Some perspectives of the application of $\text{Na}_3\text{RE}_9\text{O}_3(\text{BO}_3)_8$ oxyborates

As was shown above, the new family of sodium rare-earth oxyborates, $\text{Na}_3\text{RE}_9\text{O}_3(\text{BO}_3)_8$, have a structure belonging to the non-centrosymmetric group *P*-62*m*, which permits assuming that they have NLO properties. In the case of $\text{Na}_3\text{La}_9\text{O}_3(\text{BO}_3)_8$, we observed a second-harmonic generation (SGH) effect, which was measured by the powder technique [45]. This was confirmed by the results of Zhang et al. [46] published during the preparation of the present work. These authors found $\text{Na}_3\text{La}_9\text{O}_3(\text{BO}_3)_8$ to exhibit an optical SHG effect exceeding about 3–5 times that of KH_2PO_4 (KDP), which revealed a significant potential of the material for applications of laser frequency conversion in the blue-green wavelength range.

The remaining isostuctural $\text{Na}_3\text{RE}_9\text{O}_3(\text{BO}_3)_8$ oxyborates might prove not less promising as, say, luminescent materials or self-frequency-doubling (SFD) laser hosts.

4. Regions of phase crystallization in the ternary system Na_2O – Al_2O_3 – B_2O_3 and conditions of single-crystal growth of the oxyborate $\text{Na}_2\text{Al}_2\text{O}(\text{BO}_3)_2$ from high-temperature solutions of this system

The interest in double borates of alkaline metals and aluminum increased during the past years after it was discovered that the oxyborate $\text{K}_2\text{Al}_2\text{O}(\text{BO}_3)_2$ (KABO) crystals are a very promising NLO material for frequency conversion of high-power solid-state ultraviolet (UV) lasers [47–49]. The data available in the literature concerning double-sodium aluminum borates are rather scarce. Investigating melts of the pseudobinary system NaBO_2 – Al_2O_3 , Samedov et al. [50] first established the formation

of a compound with the composition $\text{Na}_2\text{Al}_2\text{B}_2\text{O}_7$ (Na_2O : Al_2O_3 : B_2O_3 = 1:1:1). The short communication contains a poor X-ray powder diffraction pattern of the compound which has not been indexed. According to the authors, $\text{Na}_2\text{Al}_2\text{B}_2\text{O}_7$ melts congruently at 1010 ± 10 °C. In another paper [51] some of the same authors have confirmed the results in Ref. [50] concerning $\text{Na}_2\text{Al}_2\text{B}_2\text{O}_7$ and, studying the section of $\text{Na}_2\text{O} \cdot 2\text{B}_2\text{O}_3$ – Al_2O_3 , have established the existence of a second ternary borate, NaAlB_2O_5 (Na_2O : Al_2O_3 : B_2O_3 = 1:1:2), with a melting point of 1025 ± 10 °C.

The structure of $\text{Na}_2\text{Al}_2\text{B}_2\text{O}_7$ was determined for the first time in 2000 by Corbel and Leblanc [52]. They found the compound, defined by them as oxyborate, $\text{Na}_2\text{Al}_2\text{O}(\text{BO}_3)_2$, to be isostructural with $\text{Na}_2\text{Ga}_2\text{O}(\text{BO}_3)_2$ and to crystallize in the trigonal system (S.G. *P*31*c*; *Z* = 2). More recently, the structure of $\text{Na}_2\text{Al}_2\text{O}(\text{BO}_3)_2$ was refined by He et al. [53,54], while Corbel et al. [21] established a sodium ionic conduction in this oxyborate.

According to the data available in the literature, the system Na_2O – Al_2O_3 – B_2O_3 has not yet been investigated with respect to the possibilities and conditions of growth of ternary borate single crystals. Prognostication of such possibilities and conditions was one of the principal tasks of our studies. The importance of any information of that kind increases on the background of some results reported during the preparation of this paper. They show that substitution of up to 60% of Na for K in $\text{K}_2\text{Al}_2\text{O}(\text{BO}_3)_2$ (KABO) may result in a NLO material that seems to be more promising than KABO [55]. On the other hand, doping with 3*d* metal ions which partially replace the Al^{3+} ions in $\text{Na}_2\text{Al}_2\text{O}(\text{BO}_3)_2$ could result in the formation of single crystals appropriate for application as solid-state laser hosts.

4.1. Determination of phase crystallization regions in the Na_2O – Al_2O_3 – B_2O_3 system

The temperature and concentration regions of crystallization of the different phases in the system Na_2O – Al_2O_3 – B_2O_3 were determined on the basis of the results obtained during slow cooling and spontaneous crystallization of numerous homogeneous high-temperature solutions with various compositions. In contrast with the investigations on the products of solid-state interactions between the components or the use of data from the thermal analysis (DTA and TGA) of suitable samples, the method in question has the advantage of facilitating a faster and more reliable reaching of the thermodynamic equilibrium. In addition, along with data on the crystallization regions, information is also obtained on a series of properties of the solutions (viscosity, creeping, evaporation, homogeneity degree, etc.), which are very important for the processes of single-crystal growth from these solutions.

The experiments were carried out in vertical resistance furnaces ensuring maintenance of temperature with an accuracy of ± 1 °C (Eurotherm controller). The solution

containers were cylindrical platinum crucibles with a height of 40 mm and a diameter of 40 mm. The solutions used had a mass of 50–70 g, which corresponded to a layer of about 20–25 mm thickness in the crucible. They were prepared from Na_2CO_3 , Al_2O_3 and H_3BO_3 in preset molar ratios. In order to avoid losses due to sprinkling, a mechanical mixture of Na_2CO_3 and H_3BO_3 was at first melted and decomposed in the crucibles, and only after the formation of a clear solution, the necessary amount of Al_2O_3 was added in small portions. After that the solution was homogenized with continuous stirring using a Pt stirrer at a temperature exceeding by 50–100 °C the expected crystallization temperature, T_{cryst} . The homogenization continued until a thoroughly transparent solution was obtained, which usually was achieved in 2–6 h. After that the solution temperature was gradually decreased within 1 h down to values exceeding T_{cryst} by 5–10 °C only.

The high-temperature solutions of the system Na_2O – Al_2O_3 – B_2O_3 have a high viscosity and a very pronounced trend to glass formation. For that reason, to achieve the most precise determination of T_{cryst} we ensured: (i) an appropriate temperature distribution in the solution with clearly expressed (about 10 °C) axial and radial temperature differences, resulting in a position of the surface center in the coldest zone; (ii) crystallization in a dynamic regime on a platinum disc (diameter 10–15 mm) rotating on the solution surface with a speed of 20–30 rpm and (iii) introduction, with each temperature change, of a small amount of fine powder from pre-synthesized $\text{Na}_2\text{Al}_2\text{O}(\text{BO}_3)_2$ to the solution surface. This was made at every 2–3 h with a step of 1–2 °C. The purpose was to introduce of a seed to initiate the crystallization process.

Special experiments showed that, as a result of neglecting the above requirements, the larger part of the solutions did not crystallize or the crystallization proceeded with a significant supersaturation at temperatures lower than the real T_{cryst} by 50–100 °C. The necessity of observing the above requirements in order to determine T_{cryst} with sufficient exactness is confirmed by the fact that when the temperature at which crystallization begins is maintained constant for 1–2 days, the mass of the crystals formed on the rotating disc seldom exceeds 1 g.

In each composition of the high-temperature solution the crystals obtained at T_{cryst} during slow cooling were cleaned by water treatment and part of them were characterized by X-ray phase determination. The composition of the solution was then altered in the desired direction with the appropriate step by addition of Na_2CO_3 , Al_2O_3 , or H_3BO_3 or of two of these components simultaneously and the procedure of T_{cryst} determination and phase characterization of the crystals was repeated. After 5–6 successive changes of the composition, a new solution was prepared from the initial reagents in order to minimize the errors associated with possible losses due to evaporation, decrease of the total mass that turned to crystals, etc.

The study was restricted to solution compositions where the viscosity was not unusually high, the creeping trend was

absent and the crystallization was not accompanied by noticeable losses due to evaporation. The contents of the three solution components varied between 20 and 55 mol% for Na_2O , 0 and 35 mol% for Al_2O_3 and 25 and 55 mol% for B_2O_3 . Determination of the crystallization regions of the phases in the solution Na_2O – Al_2O_3 – B_2O_3 within the above concentration limits required investigation of about 50–60 different solutions distributed inhomogeneously, according to the importance of the corresponding portion of the system.

The thermal behaviour of some characteristic samples was studied by obtaining their DTA and TGA curves using a Stanton Redcroft STA 760 instrument. Microprobe analysis with a JEOL SUPERPROBE 733 apparatus was used in experiments determining the melting characteristics of $\text{Na}_2\text{Al}_2\text{O}(\text{BO}_3)_2$.

The experimentally determined regions of phase crystallization in the investigated part of the ternary system Na_2O – Al_2O_3 – B_2O_3 are presented in Fig. 7. Regions of one binary, two ternary and one quaternary oxide are visible as follows:

- (i) Al_2O_3 crystallizing at high concentrations of this oxide in the solutions;
- (ii) NaBO_2 , at Al_2O_3 concentrations ranging from 0 to 21 mol% and temperatures from 966 °C (melting point of the compound) to about 800 °C;
- (iii) NaAlO_2 , at low B_2O_3 concentrations and an Al_2O_3 content above 27.5 mol%;
- (iv) $\text{Na}_2\text{Al}_2\text{O}(\text{BO}_3)_2$ at an Al_2O_3 concentration between 21 and 33 mol% and a temperature of 800–970 °C.

The nature of the phases crystallizing in each of the four regions is confirmed by the X-ray diffraction patterns of ground crystals grown in these regions, which completely correspond with the data available in the literature concerning the compounds under consideration. No crystallization

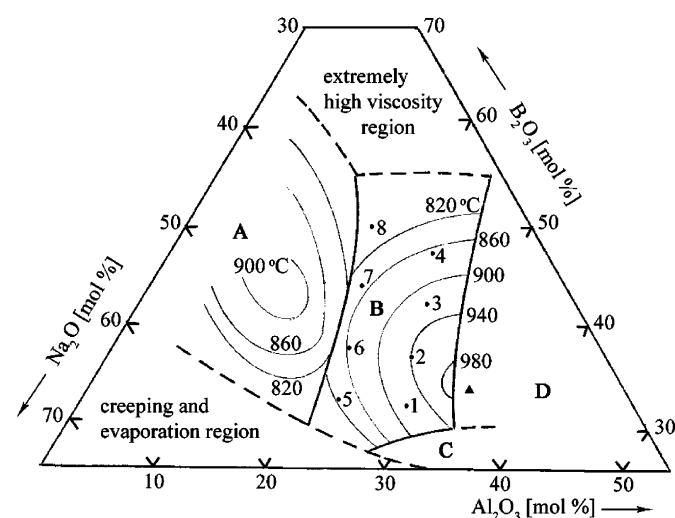


Fig. 7. Crystallization regions of the phases: NaBO_2 (A), $\text{Na}_2\text{Al}_2\text{O}(\text{BO}_3)_2$ (B), NaAlO_2 (C), and Al_2O_3 (D) in the system Na_2O – Al_2O_3 – B_2O_3 ; ▲, $\text{Na}_2\text{Al}_2\text{O}(\text{BO}_3)_2$ stoichiometric composition.

region of the double-borate NaAlB_2O_5 reported in the paper of Abdullaev et al. [51] has been established.

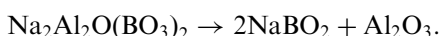
According to the literature data cited above, $\text{Na}_2\text{Al}_2\text{O}(\text{BO}_3)_2$ has a congruent character of melting. Abdullaev et al. [51] have mentioned 1010 °C as a melting point, whereas He et al. [53] are of the opinion, on the basis of the DTA curve of $\text{Na}_2\text{Al}_2\text{O}(\text{BO}_3)_2$, that this temperature is 986 °C. However, the crystallization region of the double oxyborate determined in this study lies to the left of the point for the stoichiometric molar composition of the compound ($\text{Na}_2\text{O}:\text{Al}_2\text{O}_3:\text{B}_2\text{O}_3 = 33.3:33.3:33.3$) although the upper boundary of the region ($\text{Na}_2\text{O}:\text{Al}_2\text{O}_3:\text{B}_2\text{O}_3 = 34.3:31.5:34.2$) is rather close to this composition. In other words, the results obtained indicate that $\text{Na}_2\text{Al}_2\text{O}(\text{BO}_3)_2$ should be incongruently melting, its composition in the peritectic point being close to the stoichiometric.

The choice of a method for growing $\text{Na}_2\text{Al}_2\text{O}(\text{BO}_3)_2$ single crystals requires explicit elucidation of the character of melting of this compound. In this connection, additional experiments were performed. At first DTA curves of $\text{Na}_2\text{Al}_2\text{O}(\text{BO}_3)_2$ were obtained at three different heating rates. They showed a strong temperature dependence of the endothermic peak of melting on the heating rate. Thus, at a heating rate of 5 °C/min the effect was observed at 993 °C, while at 10 °C/min this happened at 996 °C and at 15 °C/min, at 1001 °C. In fact, with such a small differences between the heating rates, the shift of the endothermic effect should not be substantial if the compound is congruently melting.

A much more definite answer to the question about the character of melting of the double oxyborate under consideration was obtained as a result of a series of experiments on thermal treatment at different temperatures of isolated single crystals. Microphotographs showed that after heating a $\text{Na}_2\text{Al}_2\text{O}(\text{BO}_3)_2$ crystal for 36 h at 968 °C it presented no change and remained transparent. No change was also observed after 10 h when the heating temperature was increased by 5 °C up to 973 °C. However, prolongation of the heat treatment at this temperature to 36 h resulted in the appearance of fine particles of another phase in the crystal. The number of these particles increased with rising temperature and prolongation of the heat treatment. Heating for 36 h at 980 °C led to the formation of particles with a hexagonal shape clearly visible in the microphotographs. The microprobe analysis and X-ray determinations indicated them to be consisting of alumina.

When the temperature of heat treatment of the $\text{Na}_2\text{Al}_2\text{O}(\text{BO}_3)_2$ crystals is increased to 1050 °C, the product becomes a fully opaque glass due to dispersed Al_2O_3 particles. In contrast to this glass, the compositions in the crystallization region of the compound (region B in Fig. 7) form colourless transparent and homogeneous glasses after quick cooling.

The explicit conclusion from the above experiments is that $\text{Na}_2\text{Al}_2\text{O}(\text{BO}_3)_2$ is a compound which, when melted, decomposes peritectically according to the reaction:



Decomposition occurs at $T = 970 \pm 3$ °C. However, since the transition needs formation of Al_2O_3 nuclei, which is a relatively slow process, the effect on the DTA curve is somewhat retarded and appears at a temperature increasing with the heating rate at which the curve has been registered. The second endothermic peak expected as a result of the peritectic decomposition, which would correspond to the complete dissolution of Al_2O_3 (the so-called liquidus point) would not be observed due to the very high temperature of location of this point (probably above 1200 °C) when also processes of intense evaporation of Na_2O and B_2O_3 begin.

A characteristic feature of most of the borate single crystals is their pronounced tendency to split in the plane perpendicular to the *c*-axis and to form hexagonal pinacoids with a small thickness. A habit of that kind creates serious problems especially with respect to the growth of single crystals with practical application. For that reason, simultaneously with the determination of the regions of phase crystallization in the system, we had to pay attention to the habit of spontaneously growing crystals of $\text{Na}_2\text{Al}_2\text{O}(\text{BO}_3)_2$ in different zones of its crystallization region. Observations on the crystals obtained from compositions in the crystallization region which correspond to points 1–8 of the diagram in Fig. 7 show that the composition of the high-temperature solution strongly affects the habit of the grown crystals. With rising B_2O_3 content in the solution, the crystals become increasingly thinner and when this content exceeds 45 mol%, the habit becomes mica-like. The drop of T_{cryst} also makes the crystals thinner but in this case the trend is much less pronounced.

4.2. Conditions of growth of $\text{Na}_2\text{Al}_2\text{O}(\text{BO}_3)_2$ single crystals

As was shown above, $\text{Na}_2\text{Al}_2\text{O}(\text{BO}_3)_2$ melts incongruently, which makes high-temperature solution growth most appropriate for obtaining single crystals. In this connection the choice of a solvent is of special importance. This choice should be based on analysis of characteristics such as width of the oxyborate concentration and temperature crystallization regions in the potential solvents, change in supersaturation degree of the solutions with decreasing temperature, temperature and concentration dependences of the solution viscosity and density, evaporation losses, etc. [56].

4.2.1. Solvents of $\text{Na}_2\text{Al}_2\text{O}(\text{BO}_3)_2$ from the system $\text{Na}_2\text{O}-\text{B}_2\text{O}_3$

In order to avoid crystal contamination by foreign admixtures, it is recommended to grow single crystals from high-temperature solutions whose solvents consist of components participating in the composition of the crystal to be obtained. That is why solvents of the system $\text{Na}_2\text{O}-\text{B}_2\text{O}_3$ were chosen.

From the diagram in Fig. 7 it is evident that the crystallization region of the $\text{Na}_2\text{Al}_2\text{O}(\text{BO}_3)_2$ oxyborate

does not include the point (denoted by \blacktriangle) corresponding to the stoichiometric composition of the compound. The region is situated entirely to the left of this point, in a zone of enhanced Na_2O and B_2O_3 contents with respect to the above composition, i.e. $\text{Na}_2\text{Al}_2\text{O}(\text{BO}_3)_2$ single crystals could be grown from solutions in which the ratio (in mol%) between the Na_2O and B_2O_3 components of the solvent varies between 70:30 and 30:70. The crystallization of $\text{Na}_2\text{Al}_2\text{O}(\text{BO}_3)_2$ with decreasing temperature is accompanied by a composition change of the solutions along the a , b , c , d and e lines for 70:30, 60:40, 50:50, 40:60 and 30:70 solvents, respectively, as shown in Fig. 8. The experimentally obtained data on the widths of the concentration and temperature crystallization regions of $\text{Na}_2\text{Al}_2\text{O}(\text{BO}_3)_2$ and the mean supersaturation (expressed as grams of substance precipitated during cooling of 100 g solution by 1°C) of solutions based on the above solvents are shown in Table 12. It can be seen that both the concentration and temperature regions where $\text{Na}_2\text{Al}_2\text{O}(\text{BO}_3)_2$ crystallizes from solutions of all the five solvents are broad enough, i.e. on this basis each of them would be suitable for the growth of the oxyborate single crystals. However, it is obvious that the saturation temperatures of the solutions in 30:70, 40:60

and 70:30 solvents are rather low. This, along with the high concentrations of B_2O_3 when 30:70 and 40:60 solvents are used, would lead to crystal growth in solutions with too high viscosities and all the inconveniences resulting from this circumstance. With the solutions of the above three solvents the lowest supersaturation values are observed, i.e. the same solution amount would give the lowest yield. The unfavourable prognosis with respect to the use of these solutions was pointed out above in connection with the habit of the crystals grown by spontaneous crystallization. Of the remaining two solvents, the one with an equimolar ratio between Na_2O and B_2O_3 , i.e. the ratio in the $\text{Na}_2\text{Al}_2\text{O}(\text{BO}_3)_2$ oxyborate, was preferred for the further investigations.

4.2.2. Solubility of $\text{Na}_2\text{Al}_2\text{O}(\text{BO}_3)_2$ in the solvent where $\text{Na}_2\text{O}:\text{B}_2\text{O}_3 = 50:50$ (NaBO_2)

The solubility of $\text{Na}_2\text{Al}_2\text{O}(\text{BO}_3)_2$ in NaBO_2 was investigated by determining the saturation temperature in solutions with preset concentration and a mass of 50–70 g each, cylindrical platinum crucibles with a height of 40 mm and a diameter of 40 mm being used as containers. The experiments were carried out in vertical resistance furnaces ensuring maintenance of temperature with an accuracy of $\pm 1^\circ\text{C}$ (Eurotherm controller).

In order to determine the saturation temperature of a given solution, in the bulk of this solution one had to achieve temperature differences that would lead to crystallization of $\text{Na}_2\text{Al}_2\text{O}(\text{BO}_3)_2$ in the centre of the solution surface. There a platinum disc, 15–20 mm in diameter, rotating continuously with a speed of 20 rpm was placed. In the above dynamic regime the crystals appeared and grew on the disc. Nucleation was initiated by introducing a very small amount of fine powder of pre-synthesized $\text{Na}_2\text{Al}_2\text{O}(\text{BO}_3)_2$ to the solution surface. The particles of this powder were dissolved when under the experimental conditions the solution temperature exceeded the saturation temperature. When the solution temperature was lower than the saturation temperature, the powder particles became centres of nucleation and growth of the oxyborate crystals. Thus, using careful periodic temperature decrease, it was possible to reach temperature values at which slow growth of a group of small crystals began. Then the solution and the crystals on the rotating disc were allowed to stand at this temperature for 1–2 days until

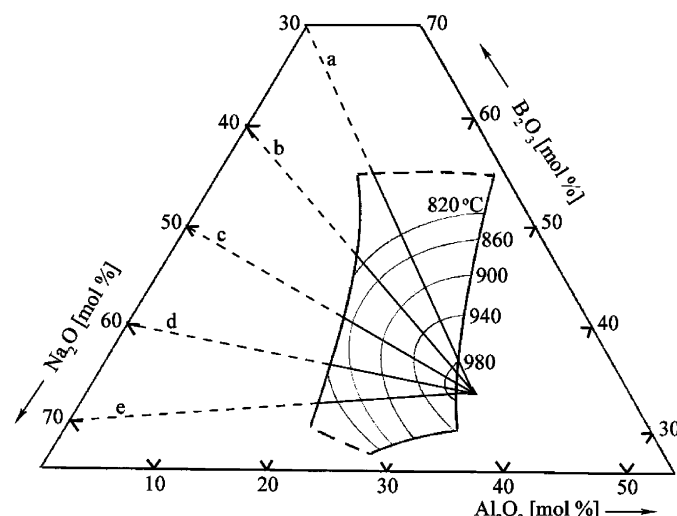


Fig. 8. Crystallization region of $\text{Na}_2\text{Al}_2\text{O}(\text{BO}_3)_2$ in the system $\text{Na}_2\text{O}-\text{Al}_2\text{O}_3-\text{B}_2\text{O}_3$ and composition change of its solutions in solvents with a $\text{Na}_2\text{O}:\text{B}_2\text{O}_3$ molar ratio of: (a) 70:30; (b) 60:40; (c) 50:50; (d) 40:60; (e) 30:70.

Table 12

Width of the crystallization regions of $\text{Na}_2\text{Al}_2\text{O}(\text{BO}_3)_2$ and supersaturation of its solutions in different solvents of the system $\text{Na}_2\text{O}-\text{B}_2\text{O}_3$

Solvent $\text{Na}_2\text{O}:\text{B}_2\text{O}_3$ (mol%)	Maximum $\text{Na}_2\text{Al}_2\text{O}(\text{BO}_3)_2$ concentration (mol%) vs. saturation temperature ($^\circ\text{C}$)	Maximum $\text{Na}_2\text{Al}_2\text{O}(\text{BO}_3)_2$ concentration (mol%) vs. saturation temperature ($^\circ\text{C}$)	$\text{Na}_2\text{Al}_2\text{O}(\text{BO}_3)_2$ concentration region width (mol%)	$\text{Na}_2\text{Al}_2\text{O}(\text{BO}_3)_2$ temperature region width (mol%)	Supersaturation (g/ $^\circ\text{C}$ per 100 g solution)
30:70	91/980	40/760	51	220	0.36
40:60	93/985	48/810	45	175	0.45
50:50	94.5/990	54/850	40.5	140	0.66
60:40	96/985	60/835	36	150	0.62
70:30	97/985	61/800	35	185	0.44

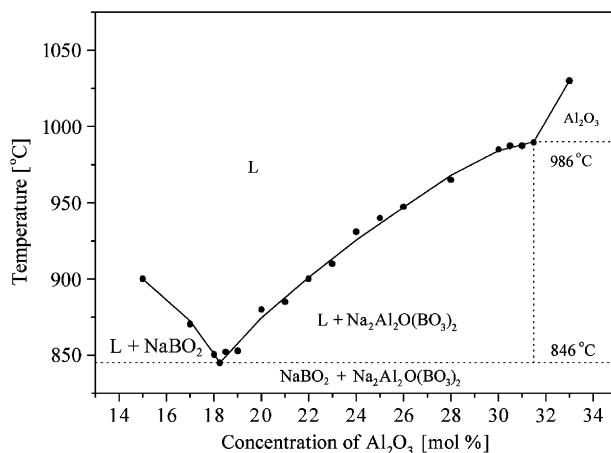


Fig. 9. NaBO_2 – Al_2O_3 section of the system Na_2O – Al_2O_3 – B_2O_3 .

equilibrium was achieved. After that the above procedure was repeated with solutions of higher $\text{Na}_2\text{Al}_2\text{O}(\text{BO}_3)_2$ concentrations, which were reached by addition of the corresponding amount of Al_2O_3 . Within the crystallization region the saturation temperature was determined for solutions whose concentration was varied by a step of 1 mol% Al_2O_3 , corresponding to 3 mol% $\text{Na}_2\text{Al}_2\text{O}(\text{BO}_3)_2$.

The results obtained during the investigation on the solubility of $\text{Na}_2\text{Al}_2\text{O}(\text{BO}_3)_2$ in NaBO_2 are illustrated by the NaBO_2 – Al_2O_3 section of the Na_2O – Al_2O_3 – B_2O_3 system (Fig. 9). It is obvious that the crystallization region of the oxyborate lies to the right of the eutectic NaBO_2 – $\text{Na}_2\text{Al}_2\text{O}(\text{BO}_3)_2$ appearing at an Al_2O_3 concentration of 18.2 mol% (or $18.2 \times 3 = 54.6$ mol% $\text{Na}_2\text{Al}_2\text{O}(\text{BO}_3)_2$), and a temperature of 985 °C. To the left of the eutectic crystallization of NaBO_2 proceeds, while Al_2O_3 crystallizes to the right of the peritectic. The calculated mean supersaturation of the solution is 0.66 g/°C per 100 g solution. With rising temperature ($\text{Na}_2\text{Al}_2\text{O}(\text{BO}_3)_2$ concentration, respectively), the supersaturation sharply increases. Thus, at 880–890 °C the supersaturation is 0.45, at 940–950 °C it is 1.15, and at 970–980 °C it reaches 3.46 g/°C per 100 g solution.

4.2.3. Viscosity and density of the solutions

The viscosity of a series of solutions of the NaBO_2 – Al_2O_3 system in the crystallization regions of $\text{Na}_2\text{Al}_2\text{O}(\text{BO}_3)_2$ was determined by a method described in previous papers [57,58]. The principle of the method consists in measuring the resistance exercised by the solution on a platinum disc rotating in it, which is determined by the solution viscosity. The power applied to the motor rotating the disc was used as quantitative measure of the resistance. The measurements were performed in a platinum crucible, 40 mm in diameter, which contained a 15–20 mm layer of the corresponding solution. The Pt disc immersed in the high-temperature solution had a diameter of 20 mm and a thickness of 1 mm. The rotating power of the disc was measured at several temperatures above the saturation

temperature and at the saturation temperature of each of the solutions. The device used for measuring the viscosity was calibrated with pure glycerol at temperatures ranging from 5 to 40 °C and a series of glycerol–water solutions at 25 °C. Precise data on the viscosity values of these calibrating liquids can be found in the literature [59]. Error estimation showed a possibility of viscosity determination by the above method with an accuracy of about $\pm 2\%$.

The densities of the solutions whose viscosities were measured, were established optically by determining the level of a solution layer (i.e. its volume) with a preset mass. The accuracy of measurement in this case was of the order of $\pm 3\%$.

The results of viscosity measurements at the saturation temperatures of solutions with different Al_2O_3 concentrations are given in Fig. 10. Evidently, the viscosity values vary within quite large boundaries: from about 500 cP at 850 °C for a solution containing 18 mol% Al_2O_3 to 4000 cP when the solution contains 28 mol% alumina. The differences are a result of the interaction between two opposite factors. On the one hand, the increase in amount of Al_2O_3 , which is a typical glass-forming oxide, should contribute to the viscosity rise whereas the temperature increase should have the opposite effect. Obviously, the effect of the increasing alumina content is much stronger, as is confirmed by the data in Figs. 11 and 12. Fig. 11 shows how the viscosity is affected by the temperature change with solutions containing 18–28 mol% Al_2O_3 (54 and 84 mol% $\text{Na}_2\text{Al}_2\text{O}(\text{BO}_3)_2$, respectively). The expected viscosity drop with rising temperature is observed. However, the other figure (Fig. 12) demonstrates a dramatic increase in viscosity with increasing alumina content in the solution, the temperature remaining constant.

The studies on the density of saturated solutions of $\text{Na}_2\text{Al}_2\text{O}(\text{BO}_3)_2$ in NaBO_2 and the density changes with rising Al_2O_3 (oxyborate, respectively) concentration indicate such changes within relatively narrow limits. Thus, at 850 °C and with an Al_2O_3 content in the solution amounting to 18 mol%, the density is 2.28 g/cm³, to decrease to 1.94 g/cm³ for a solution containing 30 mol%

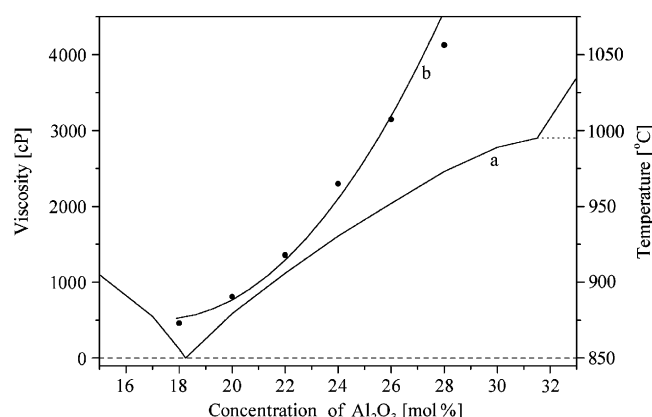


Fig. 10. Viscosity of the saturated solutions of $\text{Na}_2\text{Al}_2\text{O}(\text{BO}_3)_2$ in NaBO_2 : (a) liquidus line of the section in Fig. 9; (b) viscosity.

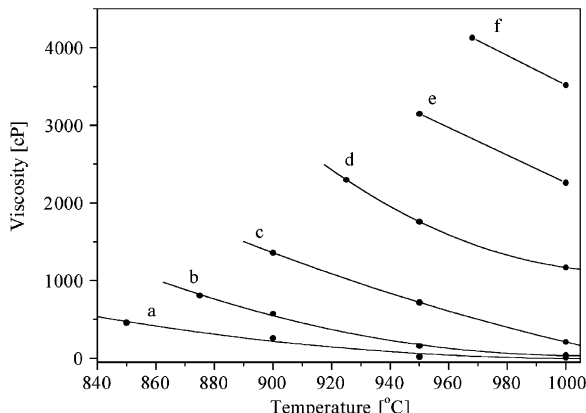


Fig. 11. Viscosity vs. temperature in solutions with a constant concentration of $\text{Na}_2\text{Al}_2\text{O}(\text{BO}_3)_2$: (a) 54 mol% (18 mol% Al_2O_3); (b) 60 mol% (20 mol% Al_2O_3); (c) 66 mol% (22 mol% Al_2O_3); (d) 72 mol% (24 mol% Al_2O_3); (e) 78 mol% (26 mol% Al_2O_3); (f) 84 mol% (28 mol% Al_2O_3).

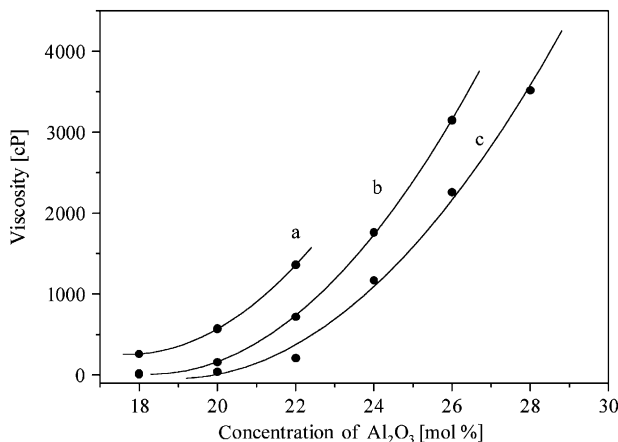


Fig. 12. Viscosity vs. $\text{Na}_2\text{Al}_2\text{O}(\text{BO}_3)_2$ concentration at a constant temperature of (a) 900 °C; (b) 950 °C and (c) 1000 °C.

Al_2O_3 , which is saturated at 980 °C. These values are lower than the theoretical density of $\text{Na}_2\text{Al}_2\text{O}(\text{BO}_3)_2$, which is 2.532 g/cm³ [53], this permitting the conclusion that the method of crystal growth from a high-temperature solution on a seed situated on the solution surface will prove appropriate for the preparation of single crystals of this oxyborate.

4.2.4. Analysis of the results

Some principal conclusions concerning the practice of growing $\text{Na}_2\text{Al}_2\text{O}(\text{BO}_3)_2$ single crystals from high-temperature solutions can be drawn on the basis of the above results.

First of all, this provides evidence that of all possible solvents of the $\text{Na}_2\text{O}-\text{B}_2\text{O}_3$ system, NaBO_2 is the most suitable. This solvent proposes very large concentration and temperature regions of crystallization of $\text{Na}_2\text{Al}_2\text{O}(\text{BO}_3)_2$ along with a sufficiently high supersaturation degree of the solutions, which ensures a high yield of crystals with a habit suitable for practical application. With solvents of a higher Na_2O content the solution supersaturation is lower

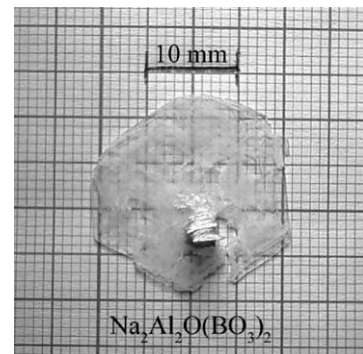


Fig. 13. A $\text{Na}_2\text{Al}_2\text{O}(\text{BO}_3)_2$ single crystal grown by TSSG with slow cooling.

and the increase in B_2O_3 concentration in the solvent above $\text{Na}_2\text{O}:\text{B}_2\text{O}_3 = 1:1$ results not only in a supersaturation drop but also in the formation of crystals with an inappropriate habit.

The second conclusion concerns the preferred initial concentration of $\text{Na}_2\text{Al}_2\text{O}(\text{BO}_3)_2$ in the solutions used for growing its single crystals. The concentration should not exceed 78 mol% (26 mol% alumina, respectively). Due to the rather high values of the solution supersaturations (above 1 g/°C per 100 g solution) and viscosities (above 3000 cP), the successful growth of $\text{Na}_2\text{Al}_2\text{O}(\text{BO}_3)_2$ single crystals from highly concentrated solutions seems to be questionable.

The high viscosity values found with all solutions indicate that an intense dynamic regime facilitating mass transfer is needed for growing $\text{Na}_2\text{Al}_2\text{O}(\text{BO}_3)_2$ single crystals. It could be achieved either by using forced convection or by creating high temperature gradients in the solutions. This is the third principal conclusion to be drawn from the present investigation.

The above conclusions were utilized for performing a preliminary experiment for the growth of a $\text{Na}_2\text{Al}_2\text{O}(\text{BO}_3)_2$ single crystal using the top-seeded solution growth (TSSG) technique with slow cooling. The experiment was carried out with a 60 g solution of a 78 mol% $\text{Na}_2\text{Al}_2\text{O}(\text{BO}_3)_2$ concentration. The oxyborate seed had the shape of a hexagonal pinacoid (3 × 1 mm) and the crystal grew in a direction perpendicular to the *c*-axis. The process lasted 3 days with a cooling rate of 1 °C/day. Fig. 13 shows the photograph of the single crystal obtained. This preliminary result is an indication of the possibility of growing $\text{Na}_2\text{Al}_2\text{O}(\text{BO}_3)_2$ single crystals from non-stoichiometric high-temperature solutions in spite of the rather high solution viscosity. Simultaneously, the distinct defects on the crystal confirm the necessity of intensified mass transfer and application of high-precision temperature control.

5. Conclusion

The results of this work represent a contribution to the knowledge of double oxyborates formed in the systems alkaline oxide– Me_2O_3 -type oxide–boron oxide.

The preparation conditions of three new oxyborates of the $\text{Na}_2\text{RE}_2\text{O}(\text{BO}_3)_2$ ($\text{RE} = \text{Y}$, Nd , Er) family with a monoclinic structure (S.G. $P2_1/c$) have been established and the cell parameters of the compounds have been determined. Their behaviour during melting has been studied and some conclusions about the appropriate methods for single-crystal growth of these substances have been drawn with a view to their use as optical materials.

It has been shown that the oxyborate $\text{Na}_2\text{La}_2\text{O}(\text{BO}_3)_2$ cannot be synthesized as a pure phase by solid-state reaction of a stoichiometric mixture of oxides. The products always contain $\text{Na}_3\text{La}_2(\text{BO}_3)_3$ and LaBO_3 as additional phases and thermal treatment at $950\text{--}1050\text{ }^\circ\text{C}$ leads to the appearance of an unknown phase whose amount becomes significant after melting. The composition of this phase corresponds to a new oxyborate of sodium and lanthanum with the formula $\text{Na}_3\text{La}_9\text{O}_3(\text{BO}_3)_8$. This compound was obtained as a pure phase during solid-state interaction between the constituent oxides at $1000\text{--}1100\text{ }^\circ\text{C}$ and its single crystals were grown by spontaneous crystallization from melts. Single-crystal X-ray data were used for determining the crystal structure of $\text{Na}_3\text{La}_9\text{O}_3(\text{BO}_3)_8$. A hexagonal unit cell (S.G. $P-62m$, $Z = 1$) with $a = 8.9033(3)\text{ \AA}$, $c = 8.7131(3)\text{ \AA}$ and $V = 598.14\text{ \AA}^3$ was found. The structure is characterized by alternate stacking along the c -axis of $\text{Na}-\text{B}-\text{O}-$, $\text{B}-\text{O}-$, $\text{La}-$ and $\text{La}-\text{O}$ -containing layers with a mirror plane at $z = \frac{1}{2}$. A framework of La_9O_3 rings and rows of BO_3 triangles running along the c -direction is established. Each La_9O_3 ring is constituted of three La_4O tetrahedra sharing a common La corner. The presence in the structure of oxygen atoms surrounded by lanthanum atoms only justifies the oxyborate label of the compound.

The oxyborate $\text{Na}_3\text{La}_9\text{O}_3(\text{BO}_3)_8$ is the forefather of a new family of isostructural $\text{Na}_3\text{RE}_9\text{O}_3(\text{BO}_3)_8$ compounds. Such compounds where $\text{RE} = \text{Nd}$, Sm and Eu were synthesized for the first time and their cell parameters were determined. The structural peculiarities of the newly obtained compounds permit the assumption that they could be the basis of advanced optical materials. This assumption has already found confirmation by the results of some preliminary studies on their properties.

Using the results of a study on spontaneous crystallization of the phases in different high-temperature solutions of the ternary system $\text{Na}_2\text{O}-\text{Al}_2\text{O}_3-\text{B}_2\text{O}_3$ we determined the concentration and temperature regions of crystallization of the double-oxyborate $\text{Na}_2\text{Al}_2\text{O}(\text{BO}_3)_2$. This compound was found to melt incongruently at $970 \pm 3\text{ }^\circ\text{C}$, which makes growth from a high-temperature solution the most appropriate method for obtaining its single crystals. According to the studies performed, the most suitable solvent is NaBO_2 . On the basis of the data on the solubility of $\text{Na}_2\text{Al}_2\text{O}(\text{BO}_3)_2$ in this solvent and the viscosity and density dependences of the solutions on the temperature and the oxyborate concentration, an optimum composition of the initial high-temperature solution for the growth of single crystals is proposed. The validity of this

choice is demonstrated by the growth on a seed using the TSSG technique and slow cooling of the solution. Recommendations are made concerning the improvement of the growth process with a view to obtaining good-quality crystals.

References

- [1] W.H. Zachariasen, G.E. Ziegler, Z. Kristallogr. 83 (1932) 354–361.
- [2] W.H. Zachariasen, Z. Kristallogr. 76 (1931) 289–293;
- W.H. Zachariasen, Z. Kristallogr. 98 (1937) 266–274.
- [3] W.H. Zachariasen, J. Chem. Phys. 5 (1937) 919–922.
- [4] V.M. Goldschmidt, H. Hauptmann, Nachr. Ges. Wiss. Göttingen, Math.-Phys. Klasse (1932) 53–72.
- [5] S.-M. Fang, Z. Kristallogr. 99 (1938) 1–8.
- [6] S.K. Filatov, R.S. Bubnova, Phys. Chem. Glass. 41 (2000) 216–224.
- [7] P. Becker, Z. Kristallogr. 216 (2001) 523–533.
- [8] P. Becker, Adv. Mater. 10 (1998) 979–992.
- [9] D.A. Keszler, Curr. Opin. Solid State Mater. Sci. 4 (1999) 155–162.
- [10] T. Sasaki, Y. Mori, M. Yoshimura, Y.K. Yap, T. Kamimura, Mater. Sci. Eng. R 30 (2000) 1–54.
- [11] G. Aka, F. Mougel, A. Khan-Harari, D. Vivien, J.M. Benitez, F. Salin, D. Pelenc, F. Balembois, P. Georges, A. Brun, N. Le Nain, M. Jacquet, J. Alloy Compd. 303–304 (2000) 401–408.
- [12] C. Chen, Z. Lin, Z. Wang, Appl. Phys. B, Lasers Opt. 80 (2005) 1–25.
- [13] Y. Idota, T. Kubota, A. Matsufuji, Y. Maekawa, T. Miyasaka, Science 276 (1997) 1395–1397.
- [14] J.L.C. Rowsell, J. Gaubicher, L.F. Nazar, J. Power Sources 97–98 (2001) 254–257.
- [15] J.L.C. Rowsell, L.F. Nazar, J. Mater. Chem. 11 (2001) 3228–3233.
- [16] V. Legagneur, Y. An, A. Mosbah, R. Portal, A. Le Gal La Salle, A. Verbaere, D. Guyomard, Y. Piffard, Solid State Ion. 139 (2001) 37–46.
- [17] A.I. Palos, M. Morcette, P. Strobel, J. Solid State Electrochem. 6 (2002) 134–138.
- [18] S. Okada, T. Tonuma, Y. Uebo, Y.-I. Yamaki, J. Power Sources 119–121 (2003) 621–625.
- [19] S. Yoshikado, T. Ohachi, I. Taniguchi, M. Watanabe, Y. Fujiki, Y. Onoda, Solid State Ion. 35 (1989) 377–385.
- [20] M. Pompetzki, B. Albert, Z. Anorg. Allg. Chem. 630 (2004) 2550–2553.
- [21] G. Corbel, D. Mazza, O. Bohnké, M. Leblanc, Solid State Sci. 7 (2005) 588–593.
- [22] J.P. Attfield, J.F. Clarke, D.A. Perkins, Physica B: Condens. Matter 180–181 (Part 2) (1992) 581–584.
- [23] R. Norrestam, M. Kritikos, A. Sjödin, J. Solid State Chem. 114 (1995) 311–316.
- [24] E.M. Kopnin, C. Bougerol-Chaillout, A.A. Belik, H. Schwer, G. Böttger, J. Karpinski, Physica C: Superconductivity 355 (2001) 119–125.
- [25] J.L.C. Rowsell, N.J. Taylor, L.F. Nazar, J. Am. Chem. Soc. 124 (2002) 6522–6523.
- [26] D.I. Ivanova, S.P. Pechev, V.S. Nikolov, P.D. Peshev, Bulg. Chem. Commun. 32 (2000) 409–417.
- [27] P. Gravereau, J.-P. Chaminade, S. Pechev, V. Nikolov, D. Ivanova, P. Peshev, Solid State Sci. 4 (2002) 993–998.
- [28] D. Binev, V. Nikolov, P. Peshev, J. Alloy Compd. 391 (2005) 256–261.
- [29] D. Binev, V. Nikolov, P. Peshev, J. Alloy Compd. 393 (2005) 287–291.
- [30] G. Corbel, M. Leblanc, E. Antic-Fidancev, M. Lemaître-Blaise, J. Solid State Chem. 144 (1999) 35–44.
- [31] J. Mascetti, M. Vlasse, P. Hagenmuller, J. Solid State Chem. 39 (1981) 288–293.
- [32] J. Mascetti, C. Fouassier, P. Hagenmuller, J. Solid State Chem. 50 (1983) 204–212.

[33] G. Zhang, Y. Wu, P. Fu, G. Wang, H. Liu, G. Fan, C. Chen, *J. Phys. Chem. Solids* 63 (2002) 145–149.

[34] J. Rodriguez-Carvajal, Powder Diffraction, in: Satellite Meeting of the 15th Congress of IUCr, Toulouse, France, 1990, p. 127.

[35] I.D. Brown, D. Altermatt, *Acta Crystallogr., Sect. B: Struct. Sci.* B 41 (1985) 247.

[36] G. Heymann, K. Beyer, H. Huppertz, *Z. Naturforsch.* 59b (2004) 1200–1208.

[37] Y. Zhang, Y.D. Li, *J. Alloy Compd.* 370 (2004) 99–103.

[38] R.D. Shannon, *Acta Crystallogr., Sect. A* 32 (1976) 751–767.

[39] G.M. Sheldrick, *SHELXS-86: A Program for the Solution of the Crystal Structures*, University of Göttingen, 1986.

[40] G.M. Sheldrick, *SHELXL-93: A Program for Crystal Structure Refinement*, University of Göttingen, 1993.

[41] Y. Laureiro, M.L. Veiga, J. Isasi, E. Ramos, A. Jerez, C. Pico, *J. Mater. Sci. Lett.* 10 (1991) 635–637.

[42] J.H. Lin, M.Z. Su, K. Wurst, E. Schweda, *J. Solid State Chem.* 126 (1996) 287–291.

[43] J.-P. Chaminade, P. Gravereau, V. Jubera, C. Fouassier, *J. Solid State Chem.* 146 (1999) 189–196.

[44] V. Jubera, P. Gravereau, J.-P. Chaminade, C. Fouassier, *J. Solid State Chem.* 156 (2001) 161–167.

[45] S.K. Kurtz, T.T. Perry, *J. Appl. Phys.* 39 (1968) 3798–3813.

[46] G. Zhang, Y. Wu, Y. Li, F. Chang, S. Pan, P. Fu, C. Chen, *J. Cryst. Growth* 275 (2005) e1997–e2001.

[47] Z.-G. Hu, T. Higashiyama, M. Yoshimura, Y.K. Yap, Y. Mori, T. Sasaki, *Jpn. J. Appl. Phys.* 37 (1998) L1093–L1094.

[48] N. Ye, W.R. Zeng, J. Jiang, B.C. Wu, C.T. Chen, B.H. Feng, X.L. Zhang, *J. Opt. Soc. Am. B* 17 (2000) 764–768.

[49] Z.-G. Hu, M. Yoshimura, Y. Mori, T. Sasaki, K. Kato, *Opt. Mater.* 23 (2003) 353–356.

[50] F.R. Samedov, G.K. Abdullaev, P.F. Rza-zade, Kh.K. Zeinalova, *Izv. Akad. Nauk SSSR, Neorg. Mater.* 7 (1971) 535–536.

[51] G.K. Abdullaev, P.F. Rza-zade, Kh.S. Mamedov, *Zh. Neorg. Khim.* 28 (1983) 208–211.

[52] G. Corbel, M. Leblanc, *J. Solid State Chem.* 154 (2000) 344–349.

[53] M. He, X.L. Chen, T. Zhou, B.Q. Hu, Y.P. Xu, T. Xu, *J. Alloy Compd.* 327 (2001) 210–214.

[54] M. He, L. Kienle, A. Simon, X.L. Chen, V. Duppel, *J. Solid State Chem.* 177 (2004) 3212–3218.

[55] M. He, X. Chen, H. Okudera, A. Simon, *Chem. Mater.* 17 (2005) 2193–2196.

[56] D. Elwell, H.J. Scheel, *Crystal Growth from High-Temperature Solutions*, Academic Press, London, 1975.

[57] V. Nikolov, P. Peshev, Kh. Khubanov, *J. Solid State Chem.* 97 (1992) 36–40.

[58] D.P. Shumov, M.P. Tarasov, V.S. Nikolov, *J. Cryst. Growth* 129 (1993) 635–639.

[59] *Handbook of Chemistry and Physics*, 66th ed., edited by R.C. Weast, J.M. Astle, W.H. Beyer, CRC Press Inc., Boca Raton, FL, 1985, p. D-232.